

# Highly Scalable Bayesian Geostatistical Modeling via Meshed Gaussian Processes on Partitioned Domains

Michele Peruzzi, Sudipto Banerjee and Andrew O. Finley

December 22, 2024

## Abstract

We introduce a class of scalable Bayesian hierarchical models for the analysis of massive geostatistical datasets. The underlying idea combines ideas on high-dimensional geostatistics by partitioning the spatial domain and modeling the regions in the partition using a sparsity-inducing directed acyclic graph (DAG). We extend the model over the DAG to a well-defined spatial process, which we call the Meshed Gaussian Process (MGP). A major contribution is the development of a MGPs on tessellated domains, accompanied by a Gibbs sampler for the efficient recovery of spatial random effects. In particular, the cubic MGP (Q-MGP) can harness high-performance computing resources by executing all large-scale operations in parallel within the Gibbs sampler, improving mixing and computing time compared to sequential updating schemes. Unlike some existing models for large spatial data, a Q-MGP facilitates massive caching of expensive matrix operations, making it particularly apt in dealing with spatiotemporal remote-sensing data. We compare Q-MGPs with large synthetic and real world data against state-of-the-art methods. We also illustrate using Normalized Difference Vegetation Index (NDVI) data from the Serengeti park region to recover latent multivariate spatiotemporal random effects at millions of locations. The source code is available at [github.com/mkln/meshgp](https://github.com/mkln/meshgp).

*Keywords:* Bayesian, spatial, large  $n$ , graphical models, domain partitioning, sparsity.

## 1 Introduction

Collecting large quantities of spatial and spatiotemporal data is now commonplace in many fields. In ecology and forestry, very large datasets are collected using satellite imaging and other remote sensing instruments such as LiDAR that periodically record high-resolution images. Unfortunately, clouds frequently obstruct the view, resulting in large regions with

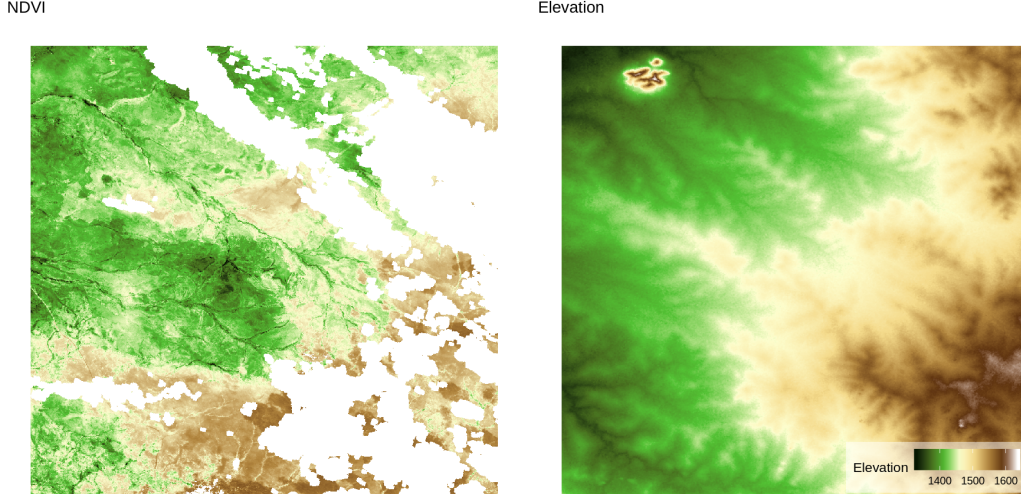


Figure 1: Left: NDVI in the Serengeti region on 2016-12-17. White areas correspond to missing data due to cloud cover. Right: elevation data for the same region.

missing information. Figure 1 shows this phenomenon using Normalized Difference Vegetation Index (NDVI) data from the Serengeti region. Filling such gaps in the data is thus an important goal, as is quantifying the associated uncertainty in predictions. This goal can be achieved via probabilistic modeling of the underlying phenomenon, which involves the specification of a spatial or spatiotemporal process that characterizes dependence among any finite set of random variables. Gaussian processes (GP) are a common, flexible choice to characterize spatial dependence, but a standard implementation is notoriously burdened by their  $O(n^3)$  computational complexity. As a consequence, intense research has been devoted in recent years to the development of scalable models for large spatial datasets – see in-depth reviews by [Sun et al. \(2011\)](#) and [Banerjee \(2017\)](#).

Computational complexity can be reduced by considering low-rank models; among these, knot-based methods motivated by kriging ideas enjoy some optimality properties but over-smooth the estimates of spatial random effects unless the number of knots is large, and require corrections to avoid overestimation of the nugget ([Banerjee et al., 2008](#); [Cressie and Johannesson, 2008](#); [Banerjee et al., 2010](#); [Guhaniyogi et al., 2011](#); [Finley et al., 2012](#)). Other methods reduce the computational burden by introducing sparsity in the covariance matrix; strategies include tapering ([Furrer et al., 2006](#); [Kaufman et al., 2008](#)) or partitioning of the spatial domain into regions with a typical assumption of independence across regions ([Sang](#)

and Huang, 2012; Stein, 2014). These can be improved by considering a recursive partitioning scheme, resulting in a multi-resolution approximation (MRA; Katzfuss 2017). Other assumptions on conditional independence assumptions also have a good track record in terms of scalability to large spatial datasets: Gaussian random Markov random fields (GMRF; Rue and Held, 2005), composite likelihood methods (Eidsvik et al., 2014), and neighbor-based likelihood approximations (Vecchia, 1988) belong to this family.

In fact, the recent literature has witnessed substantial activity surrounding the so called Vecchia approximation (Vecchia, 1988). This approximation can be looked upon as a special case of the GMRF approximations with a simplified neighborhood structure motivated from a directed acyclic graphical (DAG) representation of a Gaussian process likelihood. Extensions leading to well-defined spatial processes to accommodate inference at arbitrary locations by extending the DAG representation to the entire domain include Nearest neighbor Gaussian processes (NNGP; Datta et al. 2016a,b) and further generalizations and enhancements by constructing DAGs over the augmented space of outcomes and spatial effects (Katzfuss and Guinness, 2017). These approaches render computational scalability by introducing sparsity in the precision matrix. The DAG relies upon a specific topological ordering of the locations, which also determine the construction of the neighborhood sets, and certain orderings tend to deliver improved performance of such models (Katzfuss and Guinness, 2017; Guinness, 2018).

When inference on the latent process is sought, Bayesian inference has the benefits of providing direct probability statements based upon the posterior distribution of the process. Inference based on asymptotic approximations are avoided, but there remain challenges in computing the posterior distribution given that inference is sought on a very high-dimensional parameter space (including the realizations of the latent process). One possibility, available for Gaussian first-stage likelihoods, is to work with a collapsed or marginalized likelihood by integrating out the spatial random effects. However, Gibbs samplers and other MCMC algorithms for the collapsed models can be inexorably slow and are impractical when data are in the millions. A sequential Gibbs sampler that updates the latent spatial effects (Datta et al., 2016a) is faster in updating the parameters but suffers from high autocorrelation and slow mixing. Another possibility emerges when interest lies in prediction or imputation of the outcome variable only and not the latent process. Here, a so called “response” model that

models the outcome itself using an NNGP can be constructed. This model is much faster and enjoys superior convergence properties, but we lose inference on the latent process and its predictive performance tends to be inferior to the latent process model. Furthermore, these options are unavailable in non-Gaussian first-stage hierarchical models or when the focus is not uniquely on prediction. A detailed comparison of different approaches for computing Bayesian NNGP models is presented in [Finley et al. \(2019\)](#).

Our current contribution introduces a class of *Meshed Gaussian Process* (MGP) models for Bayesian hierarchical modeling of large spatial datasets. This class builds upon the aforementioned works that build upon [Vecchia \(1988\)](#) and other DAG based models. The inferential focus remains within the context of massive spatial datasets over very large domains. We exploit the demonstrated benefits of the DAG based models, but we now adapt them to partitioned domains. We describe dependence across regions of a partitioned domain using a small directed acyclic graph (DAG) which we refer to as a *mesh*. Within each region, some locations are selected as *reference* and collectively mapped to a single node in the DAG. Relationships among nodes are governed by kriging ideas. In the resulting Mesh Gaussian Process (MGP), regions in the spatial domain depend on each other through the reference locations. Realizations at all other locations are assumed independent, conditional upon the reference locations. This construction leads to a valid standalone spatial process.

While the idea of partitioning domains to create approximations is not new ([Katzfuss, 2017](#); [Gramacy and Lee, 2008](#)), construction of the DAG-based approximation over partitioned domains has received considerably less attention. In recent work, [Quiroz et al. \(2019\)](#) consider a similar approach in building their block-NNGP. However, the advantages of such an approach are unclear when implemented using collapsed samplers because block-NNGPs do not necessarily reduce the precision matrix fill-in. We posit that alternate graphs may be preferable when considering collapsed samplers. Crucially, collapsed samplers are impractically slow when data are in the millions. As a result, there appears to be no sizable gain in replacing NNGP models with their block version. In this regard, a major contribution, in our view, of this paper is to demonstrate the substantial scalability and performance gains when compared to state-of-the-art alternatives by considering MGPs in which domain partitioning via tessellation or tiling are coupled to similarly-patterned meshes to describe dependence across regions.

In particular, we focus on the desirable properties of MGPs based on domain tessellations when focusing on the efficient recovery of latent spatial random effects: first, they induce repeated patterns in the associated DAG that can be used to massively reduce the number of expensive matrix operations. Second, MGPs enable parallel sampling of the latent spatial random effects, promote mixing, and can be flexibly embedded in larger Bayesian hierarchical models. Finally, extensions to spatiotemporal or higher-dimensional data are straightforward once a suitable covariance function has been defined. We use axis-parallel domain partitioning coupled with cubic meshes – resulting in cubic MGPs or Q-MGPs – to show substantial improvements in computational time and inferential performance relative to other models with data sizes ranging from the thousands to the several millions, for both spatial and spatiotemporal data and using multivariate spatial processes.

The balance of this paper proceeds as follows. Section 2 introduces our general framework for hierarchical Bayesian modeling of spatial processes using networks of grouped spatial locations. The MGP is outlined in Section 3, where we provide a general, scalable computing algorithm in Section 3.1. Tessellation-based schemes and the specific case of Q-MGPs are outlined in Section 4, which highlights their properties and computational advantages. We illustrate the performance of our proposed approach in Section 5 using simulation experiments and an application on a massive dataset with millions of spatiotemporal locations. We conclude the paper with a discussion and pointers to further research. Supplementary material accompanying this manuscript as an Appendix contains further comparisons of Q-MGPs with several state-of-the-art methods for spatial data.

## 2 Spatial processes on partitioned domains

A  $q \times 1$  spatial process assigns a probability law on  $\{\mathbf{w}(\boldsymbol{\ell}) : \boldsymbol{\ell} \in \mathcal{D}\}$ , where  $\mathbf{w}(\boldsymbol{\ell})$  is a  $q \times 1$  random vector with elements  $w_i(\boldsymbol{\ell})$  for  $i = 1, 2, \dots, q$ . In the following general discussion we will not distinguish between spatial ( $\mathcal{D} \subset \mathbb{R}^d$ ) and spatiotemporal domains ( $\mathcal{D} \subset \mathbb{R}^{d+1}$ ), and denote spatial or spatiotemporal locations as  $\boldsymbol{\ell}$ ,  $\mathbf{s}$ , or  $\mathbf{u}$ .

For any finite set of spatial locations  $\{\boldsymbol{\ell}_1, \boldsymbol{\ell}_2, \dots, \boldsymbol{\ell}_{n_{\mathcal{L}}}\} = \mathcal{L} \subset \mathcal{D}$  of size  $n_{\mathcal{L}}$ , let  $P(\cdot)$  denote the probability law of the  $n_{\mathcal{L}}q \times 1$  random vector  $\mathbf{w}_{\mathcal{L}} = (\mathbf{w}(\boldsymbol{\ell}_1)^\top, \mathbf{w}(\boldsymbol{\ell}_2)^\top, \dots, \mathbf{w}(\boldsymbol{\ell}_{n_{\mathcal{L}}})^\top)^\top$  with probability density  $p(\cdot)$ . The joint density of  $\mathbf{w}_{\mathcal{L}}$  can be expressed as a DAG (or a

Bayesian network model) with respect to the ordered set of locations  $\mathcal{L}$  as

$$p(\mathbf{w}_{\mathcal{L}}) = \prod_{i=1}^{n_{\mathcal{L}}} p(\mathbf{w}(\ell_i) | \mathbf{w}(\ell_1), \dots, \mathbf{w}(\ell_{i-1})), \quad (1)$$

where the conditional set for each  $\mathbf{w}(\ell_i)$  can be interpreted as the set of its parents in a large, dense Bayesian network. Defining a simplified valid joint density on  $\mathcal{L}$  by reducing the size of the conditioning sets is a popular strategy for fast likelihood approximations in the context of large spatial datasets. One typically limits dependence to “past” neighboring locations with respect to the ordering in (1) (Vecchia, 1988; Gramacy and Apley, 2015; Stein et al., 2004; Datta et al., 2016a; Katzfuss and Guinness, 2017). The neighbors are defined and fixed and model performance may benefit from the addition of some distant locations (Stein et al., 2004). The ordering in  $\mathcal{L}$  is also fixed and inferential performance may benefit from the use of some fixed permutations (Guinness, 2018). The result of shrinking the conditional sets to a smaller set of neighbors from the past yields a sparse DAG or Bayesian network, which yields potentially massive computational gains.

We proceed in a similar manner, but instead of defining a sparse DAG at the level of each individual location, we map entire groups of locations to nodes in a much smaller graph; the same graph will be used to model the dependence between any location in the spatial domain and, therefore, to define a spatial process. Let  $\mathcal{P} = \{\mathcal{D}_1, \dots, \mathcal{D}_M\}$  be a partition of  $\mathcal{D}$  into  $M$  mutually exclusive subsets so that  $\mathcal{D} = \cup_{i=1}^M \mathcal{D}_i$  and  $\mathcal{D}_i \cap \mathcal{D}_j = \emptyset$  whenever  $i \neq j$ . Similar to the nomenclature in the NNGP, we fix a *reference set*  $\mathcal{S} = \{\mathbf{s}_1, \dots, \mathbf{s}_{n_{\mathcal{S}}}\} \subset \mathcal{D}$ , which itself is partitioned using  $\mathcal{P}$  by letting  $\mathcal{S}_j = \mathcal{D}_j \cap \mathcal{S}$ . The set of non-reference locations is similarly partitioned with  $\mathcal{U}_j = \mathcal{D}_j \setminus \mathcal{S}_j$  so that  $\mathcal{D}_j = \mathcal{S}_j \cup \mathcal{U}_j$  for each  $j = 1, 2, \dots, M$ . We now construct a DAG to model dependence within and between  $\mathcal{S}$  and  $\mathcal{U}$ . Let  $\mathcal{G} = \{\mathbf{V}, \mathbf{E}\}$  be a graph with nodes  $\mathbf{V} = \mathbf{A} \cup \mathbf{B}$ , where we refer to  $\mathbf{A} = \{\mathbf{a}_1, \dots, \mathbf{a}_M\}$  as the *reference nodes* and to  $\mathbf{B} = \{\mathbf{b}_1, \dots, \mathbf{b}_M\}$  as the *non-reference*, or simply “other”, nodes. Let  $\mathbf{A} \cap \mathbf{B} = \emptyset$ . We introduce a map  $\eta : \mathcal{D} \rightarrow \mathbf{V}$  such that

$$\eta(\ell) = \begin{cases} \mathbf{a}_j \in \mathbf{A} & \text{if } \ell \in \mathcal{S}_j \\ \mathbf{b}_j \in \mathbf{B} & \text{if } \ell \in \mathcal{U}_j \end{cases}. \quad (2)$$

This surjective many-to-one map links each location in  $\mathcal{S}_j$  and  $\mathcal{U}_j$  to a node in  $\mathcal{G}$ . The edges connecting nodes in  $\mathcal{G}$  are  $\mathbf{E} = \{\text{Pa}[\mathbf{v}_1], \dots, \text{Pa}[\mathbf{v}_{2M}]\}$  where  $\text{Pa}[\mathbf{v}] \subset \mathbf{V}$  denotes the set of

parents of any  $\mathbf{v} \in \mathbf{V}$  and, hence, identifies the directed edges pointing to  $\mathbf{v}$ . We take  $\mathcal{G}$  to be acyclic, meaning that there is no chain  $\{\mathbf{v}_{i_1} \rightarrow \mathbf{v}_{i_2} \rightarrow \dots \rightarrow \mathbf{v}_{i_t}\}$  of elements of  $\mathbf{V}$  such that  $\mathbf{v}_{i_j} \in \text{Pa}[\mathbf{v}_{i_{j+1}}]$  and  $\mathbf{v}_{i_{j+1}} \in \text{Pa}[\mathbf{v}_{i_1}]$ . Crucially, we assume that  $\text{Pa}[\mathbf{v}] \subset \mathbf{A}$  for all  $\mathbf{v} \in \mathbf{V}$ , meaning that only reference nodes have children, to distinguish the reference nodes  $\mathbf{A}$  from the other nodes  $\mathbf{B}$ . Apart from the assumption that  $\mathbf{a}_j \in \text{Pa}[\mathbf{b}_j]$ , we refrain from defining the parents of a node, thereby retaining flexibility. Later in Section 4 we will consider meshes associated to domain tessellations.

Consider the enumeration  $\mathcal{S}_i = \{\mathbf{s}_{i_1}, \dots, \mathbf{s}_{i_{n_i}}\}$ , where  $\{i_1, i_2, \dots, i_{n_i}\} \subset \{1, 2, \dots, n_{\mathcal{S}}\}$ , and let  $\mathbf{w}_i = (\mathbf{w}(\mathbf{s}_{i_1})^\top, \mathbf{w}(\mathbf{s}_{i_2})^\top, \dots, \mathbf{w}(\mathbf{s}_{i_{n_i}})^\top)^\top$  be the  $n_i q \times 1$  random vector listing elements of  $\mathbf{w}(\mathbf{s})$  for each  $\mathbf{s} \in \mathcal{S}_i$ . We now rewrite (1) as a product of  $M$  conditional densities

$$p(\mathbf{w}_{\mathcal{S}}) = p(\mathbf{w}_1, \mathbf{w}_2, \dots, \mathbf{w}_M) = \prod_{i=1}^M p(\mathbf{w}_i | \mathbf{w}_1, \dots, \mathbf{w}_{i-1}). \quad (3)$$

The conditioning sets are then reduced based on the graph  $\mathcal{G}$ :

$$\tilde{p}(\mathbf{w}_{\mathcal{S}}) = \prod_{i=1}^M p(\mathbf{w}_i | \mathbf{w}_{[i]}), \quad (4)$$

where we denote  $\mathbf{w}_{[i]} = \{\mathbf{w}_j : \mathbf{a}_j \in \text{Pa}[\mathbf{a}_i]\}$ , and  $\text{Pa}[\mathbf{a}_i] \subset \{\mathbf{a}_1, \dots, \mathbf{a}_{i-1}\} \subset \mathbf{A}$ . This is a proper multivariate joint density since the graph is acyclic (Lauritzen, 1996). It is instructive to note how the above approximation behaves when the size of the parent set shrinks, for a given domain partitioning scheme. To this end, we adapt a result in Banerjee (2020) and show that sparser DAGs correspond to a larger Kullback-Leibler (KL) divergence from the base density  $p$ . This result has been proved earlier for Gaussian likelihoods by Guinness (2018), but the argument given below is free of distributional assumptions.

Consider random vector  $\mathbf{w}$  and some partition of the domain  $\mathcal{P}$  corresponding to nodes  $\mathbf{V} = \{\mathbf{v}_1, \dots, \mathbf{v}_M\}$  via map  $\eta$ . Let the base process correspond to graph  $\mathcal{G}_0 = \{\mathbf{V}, \mathbf{E}_0\}$  where  $\mathbf{E}_0 = \{\text{Pa}_0[\mathbf{v}_1], \dots, \text{Pa}_0[\mathbf{v}_M]\}$ . Then, let  $\mathcal{G}_1 = \{\mathbf{V}, \mathbf{E}_1\}$  where  $\mathbf{E}_1 = \{\text{Pa}_1[\mathbf{v}_1], \dots, \text{Pa}_1[\mathbf{v}_M]\}$  and  $\text{Pa}_1[\mathbf{v}_i] \subseteq \text{Pa}_0[\mathbf{v}_i]$  for all  $i \in \{1, \dots, M\}$ . Finally construct  $\mathcal{G}_2 = \{\mathbf{V}, \mathbf{E}_2\}$  by letting  $\text{Pa}_2[\mathbf{v}_{i^*}] = \text{Pa}_1[\mathbf{v}_{i^*}] \setminus \{\mathbf{v}^*\}$  for some  $\mathbf{v}^* \in \text{Pa}_1[\mathbf{v}_{i^*}]$ . In other words, graph  $\mathcal{G}_2$  is obtained by removing the directed edge  $\mathbf{v}^* \rightarrow \mathbf{v}_{i^*}$  from  $\mathcal{G}_1$ . We approximate  $p$  using densities  $p_1$  and  $p_2$  based on  $\mathcal{G}_1$  and  $\mathcal{G}_2$ , respectively, obtaining

$$\frac{p_1(\mathbf{w})}{p_2(\mathbf{w})} = \prod_{i=1}^M \frac{p(\mathbf{w}_i | \mathbf{w}_{[i]_1})}{p(\mathbf{w}_i | \mathbf{w}_{[i]_2})} = \frac{p(\mathbf{w}_{i^*} | \mathbf{w}_{[i^*]_1})}{p(\mathbf{w}_{i^*} | \mathbf{w}_{[i^*]_2})}. \quad (5)$$



Considering the Kullback-Leibler divergence of each density from  $p$ , and denoting  $\mathbf{V}^* = \mathbf{V} \setminus \{\{i^*\} \cup \text{Pa}_1[i^*]\}$ , we find

$$\begin{aligned}
KL(p_2||p) - KL(p_1||p) &= \int \left\{ \log \left( \frac{p(\mathbf{w})}{p_2(\mathbf{w})} \right) - \log \left( \frac{p(\mathbf{w})}{p_1(\mathbf{w})} \right) \right\} p(\mathbf{w}) d\mathbf{w} \\
&= \int \log \left( \frac{p_1(\mathbf{w})}{p_2(\mathbf{w})} \right) p(\mathbf{w}) d\mathbf{w} = \int \log \left( \frac{p(\mathbf{w}_{i^*} | \mathbf{w}_{[i^*]_1})}{p(\mathbf{w}_{i^*} | \mathbf{w}_{[i^*]_2})} \right) p(\mathbf{w}) d\mathbf{w} \\
&= \int \log \left( \frac{p(\mathbf{w}_{i^*} | \mathbf{w}_{[i^*]_1})}{p(\mathbf{w}_{i^*} | \mathbf{w}_{[i^*]_2})} \right) p(\mathbf{w}_{i^*}, \mathbf{w}_{[i^*]_1}) d\mathbf{w}_{i^*} d\mathbf{w}_{[i^*]_1} \\
&= \int \left\{ \int \log \left( \frac{p(\mathbf{w}_{i^*} | \mathbf{w}_{[i^*]_1})}{p(\mathbf{w}_{i^*} | \mathbf{w}_{[i^*]_2})} \right) p(\mathbf{w}_{i^*} | \mathbf{w}_{[i^*]_1}) d\mathbf{w}_{i^*} \right\} p(\mathbf{w}_{[i^*]_1}) d\mathbf{w}_{[i^*]_1} \geq 0,
\end{aligned} \tag{6}$$

where we use (5), the fact that  $\mathbf{V}^*$  and  $\{i^*\} \cup \text{Pa}_1[i^*]$  are disjoint, and Jensen's inequality. This result implies that larger parent sets are preferable as they correspond to better approximations to the full model; the choice of sparser graphs will be driven by computational considerations – see Section 3.2.

We construct the spatial process over arbitrary locations by enumerating other locations as  $\mathcal{U} = \{\mathbf{u}_1, \dots, \mathbf{u}_{n_{\mathcal{U}}}\} \subset \mathcal{D} \setminus \mathcal{S}$  and extending (4) to the non-reference locations. Given the partition of  $\mathcal{U}$  defined earlier with components  $\mathcal{U}_j$  for  $j = 1, 2, \dots, M$ , for each  $\mathbf{u} \in \mathcal{U}_j$  we set  $\eta(\mathbf{u}) = \mathbf{b}_j$  and recall that  $\text{Pa}[\mathbf{b}_j] \subset \mathbf{A}$  by construction. For each  $i = 1, \dots, n_{\mathcal{U}}$ , we denote  $\mathbf{w}_{[\mathbf{u}_i]} = \{\mathbf{w}_j : \mathbf{b}_j \in \text{Pa}[\eta(\mathbf{u}_i)]\} \subset \mathbf{w}_{\mathcal{S}}$  and define the conditional density of  $\mathbf{w}_{\mathcal{U}}$  given  $\mathbf{w}_{\mathcal{S}}$  as

$$\tilde{p}(\mathbf{w}_{\mathcal{U}} | \mathbf{w}_{\mathcal{S}}) = \prod_{\mathbf{u}_i \in \mathcal{U}} p(\mathbf{w}(\mathbf{u}_i) | \mathbf{w}_{[\mathbf{u}_i]}) = \prod_{j=1}^M p(\mathbf{w}_{\mathcal{U}_j} | \mathbf{w}_{[\mathbf{b}_j]}). \tag{7}$$

Therefore, for any finite subset of spatial locations  $\mathcal{L} \subset \mathcal{D}$  we can let  $\mathcal{U} = \mathcal{L} \setminus \mathcal{S}$  and obtain

$$\tilde{p}(\mathbf{w}_{\mathcal{L}}) = \int \tilde{p}(\mathbf{w}_{\mathcal{U}} | \mathbf{w}_{\mathcal{S}}) \tilde{p}(\mathbf{w}_{\mathcal{S}}) \prod_{\mathbf{s}_i \in \mathcal{S} \setminus \mathcal{L}} d(\mathbf{w}(\mathbf{s}_i)).$$

We show (see Appendix A) that this is a well-defined process by verifying the Kolmogorov consistency conditions. This new process can be built starting from a base process, a fixed reference set, domain partition  $\mathcal{P}$  and a graph  $\mathcal{G}$ . In the next section, we use this construction for Gaussian processes.



### 3 Meshed Gaussian Processes

Let  $\{\mathbf{w}(\boldsymbol{\ell}) : \boldsymbol{\ell} \in \mathcal{D}\}$  be a  $q$ -variate multivariate Gaussian process, denoted as  $\mathbf{w}(\boldsymbol{\ell}) \sim GP(\mathbf{0}, \mathbf{C}(\cdot, \cdot | \boldsymbol{\theta}))$ . The *cross-covariance*  $\mathbf{C}(\cdot, \cdot | \boldsymbol{\theta})$  indexed by parameters  $\boldsymbol{\theta}$  is a function  $\mathbf{C} : \mathcal{D} \times \mathcal{D} \rightarrow \mathcal{M}_{q \times q}$ , where  $\mathcal{M}_{q \times q}$  is a subset of  $\mathbb{R}^{q \times q}$  (the space of all  $q \times q$  real matrices) such that the  $(i, j)$ -th entry of  $\mathbf{C}(\boldsymbol{\ell}, \boldsymbol{\ell}' | \boldsymbol{\theta})$  evaluates the covariance between the  $i$ -th and  $j$ -th elements of  $\mathbf{w}(\boldsymbol{\ell})$  at  $\boldsymbol{\ell}$  and  $\boldsymbol{\ell}'$ , respectively, i.e.,  $\text{cov}(w_i(\boldsymbol{\ell}), w_j(\boldsymbol{\ell}'))$ . We omit dependence on  $\boldsymbol{\theta}$  to simplify notation. The cross-covariance function itself needs to be neither symmetric nor positive-definite, but must satisfy the following two properties: (i)  $\mathbf{C}(\boldsymbol{\ell}, \boldsymbol{\ell}') = \mathbf{C}(\boldsymbol{\ell}', \boldsymbol{\ell})^\top$ ; and (ii)  $\sum_{i=1}^n \sum_{j=1}^n \mathbf{z}_i^\top \mathbf{C}(\boldsymbol{\ell}_i, \boldsymbol{\ell}_j) \mathbf{z}_j > 0$  for any integer  $n$  and any finite collection of points  $\{\boldsymbol{\ell}_1, \boldsymbol{\ell}_2, \dots, \boldsymbol{\ell}_n\}$  and for all  $\mathbf{z}_i \in \mathbb{R}^q \setminus \{\mathbf{0}\}$ . See [Genton and Kleiber \(2015\)](#) for a review of cross-covariance functions for multivariate processes. The (partial) realization of the multivariate process over any finite set  $\mathcal{L}$  has a multivariate normal distribution  $\mathbf{w}_{\mathcal{L}} \sim N(\mathbf{0}, \mathbf{C}_{\mathcal{L}})$  where  $\mathbf{w}_{\mathcal{L}}$  is the  $qn_{\mathcal{L}} \times 1$  column vector and  $\mathbf{C}_{\mathcal{L}}$  is the  $qn_{\mathcal{L}} \times qn_{\mathcal{L}}$  block matrix with the  $q \times q$  matrix  $\mathbf{C}(\boldsymbol{\ell}_i, \boldsymbol{\ell}_j)$  as its  $(i, j)$  block for  $i, j = 1, \dots, n_{\mathcal{L}}$ .

The construction of the MGP will start with a base, or parent, multivariate GP for  $\mathbf{w}(\boldsymbol{\ell})$  and then, using the graph  $\mathcal{G}$  defined in Section 2, represent the joint density at the reference set  $\mathcal{S}$  as

$$\tilde{p}(\mathbf{w}_{\mathcal{S}}) = \prod_{j=1}^M N(\mathbf{w}_j | \mathbf{H}_j \mathbf{w}_{[j]}, \mathbf{R}_j), \quad (8)$$

where  $\mathbf{H}_j = \mathbf{C}_{\mathcal{S}_j, \mathcal{S}_{[j]}} \mathbf{C}_{\mathcal{S}_{[j]}}^{-1}$  and  $\mathbf{R}_j = \mathbf{C}_{\mathcal{S}_j} - \mathbf{C}_{\mathcal{S}_j, \mathcal{S}_{[j]}} \mathbf{C}_{\mathcal{S}_{[j]}}^{-1} \mathbf{C}_{\mathcal{S}_{[j]}, \mathcal{S}_j}$ . The resulting joint density  $\tilde{p}(\mathbf{w}_{\mathcal{S}})$  is multivariate normal with covariance  $\tilde{\mathbf{C}}_{\mathcal{S}}$  and a precision matrix  $\tilde{\mathbf{C}}_{\mathcal{S}}^{-1}$ . The precision matrix for Gaussian graphical models is easily derived using customary linear model representations for each conditional regression. Consider the DAG in (4). Each  $\mathbf{w}_i$  is  $n_i q \times 1$  and let  $J_i = |\text{Pa}[\mathbf{a}_i]|$  be the number of parents for  $\mathbf{a}_i$  in the graph  $\mathcal{G}$ . Furthermore, let  $\mathbf{C}_{i,j}$  be the  $n_i q \times n_j q$  covariance matrix between  $\mathbf{w}_i$  and  $\mathbf{w}_j$ ,  $\mathbf{C}_{i,[i]}$  be the  $n_i q \times J_i q$  covariance matrix between  $\mathbf{w}_i$  and  $\mathbf{w}_{[i]}$ , and  $\mathbf{C}_{[i],[i]}$  be the  $J_i q \times J_i q$  covariance matrix between  $\mathbf{w}_i$  and itself. Representing each conditional density in (4) as a linear regression on  $\mathbf{w}_i$ , we get

$$\mathbf{w}_1 = \boldsymbol{\omega}_1 \sim N(\mathbf{0}, \mathbf{R}_1); \quad \mathbf{w}_i = \sum_{\{j: \mathbf{a}_j \in \text{Pa}[\mathbf{a}_i]\}} \mathbf{H}_{ij} \mathbf{w}_j + \boldsymbol{\omega}_i, \quad i = 2, 3, \dots, M, \quad (9)$$

where each  $\mathbf{H}_{ij}$  is an  $n_i q \times n_j q$  is a coefficient matrix representing the multivariate regression of  $\mathbf{w}_j$  given  $\mathbf{w}_{[i]}$ ,  $\boldsymbol{\omega}_i \stackrel{\text{ind}}{\sim} N(\mathbf{0}, \mathbf{R}_i)$  for  $i = 1, 2, \dots, M$ , and each  $\mathbf{R}_i$  is an  $n_i q \times n_i q$  residual

covariance matrix. We set  $\mathbf{H}_{ii} = \mathbf{O}$  and  $\mathbf{H}_{ij} = \mathbf{O}$ , where  $\mathbf{O}$  is the matrix of zeros, whenever  $j \in \{j : \mathbf{a}_j \notin \text{Pa}[\mathbf{a}_i]\}$ . For  $j \in \{j : \mathbf{a}_j \in \text{Pa}[\mathbf{a}_i]\}$ , let  $\{j_1, j_2, \dots, j_{J_i}\}$  be the indices in  $\text{Pa}[\mathbf{a}_i]$  and let  $\mathbf{H}_{i,[i]} = [\mathbf{H}_{i,j_1}, \mathbf{H}_{i,j_2}, \dots, \mathbf{H}_{i,j_{J_i}}]$  be the  $n_i q \times (\sum_{k=1}^{J_i} n_{j_k})q$  block matrix formed by stacking  $\mathbf{H}_{i,j_k}$  side by side for each  $\mathbf{a}_{j_k} \in \text{Pa}[\mathbf{a}_i]$ . Since  $\mathbb{E}[\mathbf{w}_i | \mathbf{w}_{[i]}] = \mathbf{H}_{i,[i]} \mathbf{w}_{[i]} = \mathbf{C}_{i,[i]} \mathbf{C}_{[i][i]}^{-1} \mathbf{w}_{[i]}$ , we obtain  $\mathbf{H}_{i,[i]} = \mathbf{C}_{i,[i]} \mathbf{C}_{[i][i]}^{-1}$  and each  $\mathbf{H}_{ij_K}$  can be obtained from the respective submatrix of  $\mathbf{H}_{i,[i]}$ . We also obtain  $\mathbf{D}_i = \text{var}\{\mathbf{w}_i | \mathbf{w}_{[i]}\} = \mathbf{C}_{i,i} - \mathbf{C}_{i,[i]} \mathbf{C}_{[i][i]}^{-1} \mathbf{C}_{[i],i}$ . Therefore, all the  $\mathbf{H}_{ij}$ 's and  $\mathbf{R}_i$ 's can be computed from the base cross-covariance function.

The distribution of  $\mathbf{w} = [\mathbf{w}_1^\top, \mathbf{w}_2^\top, \dots, \mathbf{w}_M^\top]^\top$  can be obtained by noting that  $\mathbf{w} = \mathbf{H}\mathbf{w} + \boldsymbol{\omega}$ , where  $\mathbf{H} = \{\mathbf{H}_{ij}\}$  is the  $(\sum_{i=1}^M n_i q) \times (\sum_{i=1}^M n_i q)$  block matrix with  $\{\mathbf{H}_{ij}\}$  as  $(i, j)$ -th block. Therefore,  $\tilde{\mathbf{C}}_{\mathcal{S}} = \text{var}(\mathbf{w}) = (\mathbf{I} - \mathbf{H})^{-1} \mathbf{R} (\mathbf{I} - \mathbf{H})^{-\top}$ , where  $\mathbf{R}$  is block-diagonal with  $\mathbf{R}_i$  as the  $(i, i)$ -th block. Note that  $\mathbf{I} - \mathbf{H}$  is block lower-triangular with 1's on the diagonal, hence non-singular. Also, the precision matrix  $\tilde{\mathbf{C}}_{\mathcal{S}}^{-1} = (\mathbf{I} - \mathbf{H})^\top \mathbf{R}^{-1} (\mathbf{I} - \mathbf{H})$  is sparse because of  $\mathbf{H}_{ij} = \mathbf{O}$  whenever  $\mathbf{a}_j \notin \text{Pa}[\mathbf{a}_i]$ . Block-sparsity of  $\tilde{\mathbf{C}}_{\mathcal{S}}^{-1}$  can be induced by building  $\mathcal{G}$  with few, carefully placed directed edges among nodes in  $\mathbf{A}$ ; Appendix B contains a more in-depth treatment. We extend (8) to the collection of non-reference locations  $\mathcal{U} \subset \mathcal{D} \setminus \mathcal{S}$ :

$$\tilde{p}(\mathbf{w}_{\mathcal{U}} | \mathbf{w}_{\mathcal{S}}) = \prod_{j=1}^M N(\mathbf{w}_{\mathcal{U}_j} | \mathbf{H}_{\mathcal{U}_j} \mathbf{w}_{[\mathbf{b}_j]}, \mathbf{R}_{\mathcal{U}_j}) = N(\mathbf{w}_{\mathcal{U}} | \mathbf{H}_{\mathcal{U}} \mathbf{w}_{\mathcal{S}}, \mathbf{R}_{\mathcal{U}}), \quad (10)$$

where  $\mathbf{H}_{\mathcal{U}_j} = \mathbf{C}_{\mathcal{U}_j, \mathcal{S}_{[\mathbf{b}_j]}} \mathbf{C}_{\mathcal{S}_{[\mathbf{b}_j]}}^{-1}$  and  $\mathbf{R}_{\mathcal{U}_j} = \mathbf{C}_{\mathcal{U}_j} - \mathbf{C}_{\mathcal{U}_j, \mathcal{S}_{[\mathbf{b}_j]}} \mathbf{C}_{\mathcal{S}_{[\mathbf{b}_j]}}^{-1} \mathbf{C}_{\mathcal{S}_{[\mathbf{b}_j]}, \mathcal{U}_j}$ , analogously to (8), while  $\mathbf{H}_{\mathcal{U}}$  and  $\mathbf{R}_{\mathcal{U}}$  are analogous to  $\mathbf{H}_{\mathcal{S}}$  and  $\mathbf{R}_{\mathcal{S}}$ . Clearly, given that all the  $\tilde{p}$  densities are Gaussian, all finite dimensional distributions will also be Gaussian. We have constructed a Gaussian process with the following cross-covariance function for any two locations  $\ell_1, \ell_2 \in \mathcal{D}$

$$\text{Cov}_{\tilde{p}}(\mathbf{w}(\ell_1), \mathbf{w}(\ell_2)) = \begin{cases} \tilde{\mathbf{C}}_{\mathbf{s}_i, \mathbf{s}_j} & \text{if } \ell_1 = \mathbf{s}_i, \ell_2 = \mathbf{s}_j \text{ and } \mathbf{s}_i, \mathbf{s}_j \in \mathcal{S} \\ \mathbf{H}_{\ell_1} \tilde{\mathbf{C}}_{\mathcal{S}_{[\ell_1]}, \mathbf{s}_j} & \text{if } \ell_1 \in \mathcal{D} \setminus \mathcal{S}, \ell_2 = \mathbf{s}_j \text{ and } \mathbf{s}_j \in \mathcal{S} \\ \delta_{(\ell_1 = \ell_2)} \mathbf{R}_{\ell_1} + \mathbf{H}_{\ell_1} \tilde{\mathbf{C}}_{\mathcal{S}_{[\ell_1]}, \mathcal{S}_{[\ell_2]}} \mathbf{H}_{\ell_2}^\top & \text{otherwise.} \end{cases}$$

For a given base Gaussian covariance function  $\mathbf{C}$ , domain partitioning  $\mathcal{P}$ , mesh  $\mathcal{G}$ , and reference set  $\mathcal{S}$ , we denote the corresponding mesh Gaussian process as  $\text{MGP}(\mathcal{G}, \mathcal{P}, \mathcal{S}, \mathbf{C})$ .

### 3.1 Bayesian hierarchical model and Gibbs sampler

Mesh GPs correspond to block-sparse precision matrices that are constructed cheaply from their block-sparse Cholesky factors by solving small linear systems. General purpose sparse-

Cholesky algorithms (Davis, 2006; Chen et al., 2008) can then be used to obtain collapsed samplers as in Finley et al. (2019). Unfortunately, these algorithms can only be used on Gaussian first stage models and tend to be too slow to be practically viable when data are in the millions. Hence, we develop a more general scalable Gibbs sampler for the recovery of spatial random effects in hierarchical MGP models that obviates computing with large matrices for its implementation.

Consider a linear multivariate spatiotemporally-varying regression model at  $\ell \in \mathcal{D} \subset \mathbb{R}^{d+1}$ , where

$$\mathbf{y}(\ell) = \mathbf{X}(\ell)^\top \boldsymbol{\beta} + \mathbf{Z}(\ell)^\top \mathbf{w}(\ell) + \boldsymbol{\varepsilon}(\ell), \quad (11)$$

where  $\mathbf{y}(\ell) \in \mathbb{R}^l$  is the multivariate point-referenced outcome,  $\mathbf{X}(\ell)^\top = \text{blockdiag}\{\mathbf{x}_i(\ell)^\top\}_{i=1}^l$  is a  $l \times p = l \times \sum p_i$  matrix of spatially referenced predictors linked to constant coefficients  $\boldsymbol{\beta}$ ,  $\mathbf{w}(\ell)$  is the spatial process,  $\mathbf{Z}(\ell)$  is a  $l \times q$  design matrix,  $\boldsymbol{\varepsilon}(\ell)$  is measurement error such that  $\boldsymbol{\varepsilon}(\ell) \stackrel{iid}{\sim} N(0, \mathbf{D})$  and  $\mathbf{D} = \text{diag}(\tau_1^2, \dots, \tau_l^2)$ . A simple univariate regression model with a spatially-varying intercept can be obtained with  $l = 1$ ,  $\mathbf{Z}(\ell) = 1$ . For a given set of observed locations  $\mathcal{T} = \{\ell_1, \dots, \ell_n\}$  we can write the above model compactly

$$\mathbf{y} = \mathbf{X}\boldsymbol{\beta} + \mathbf{Z}\mathbf{w} + \boldsymbol{\varepsilon},$$

where  $\mathbf{y} = (\mathbf{y}(\ell_1)^\top, \dots, \mathbf{y}(\ell_n)^\top)^\top$ ,  $\mathbf{w}$  and  $\boldsymbol{\varepsilon}$  are similarly defined,  $\mathbf{X} = [\mathbf{X}(\ell_1) : \dots : \mathbf{X}(\ell_n)]^\top$ ,  $\mathbf{Z} = \text{blockdiag}(\{\mathbf{Z}(\ell_i)^\top\}_{i=1}^n)$ , and  $\mathbf{D}_n = \text{blockdiag}(\{\mathbf{D}\}_{i=1}^n)$ .

For subsets  $\{\ell_1, \dots, \ell_{n_A}\} = \mathcal{A} \subset \mathcal{T}$ , let  $\mathbf{y}(\mathcal{A}) = (\mathbf{y}(\ell_1)^\top, \dots, \mathbf{y}(\ell_{n_A})^\top)^\top$ , with analogous definitions for  $\mathbf{w}(\mathcal{A})$  and  $\boldsymbol{\varepsilon}(\mathcal{A})$ ,  $\mathbf{X}(\mathcal{A}) = [\mathbf{X}(\ell_1) : \dots : \mathbf{X}(\ell_{n_A})]^\top$ ,  $\mathbf{Z}_{\mathcal{A}} = \text{blockdiag}(\{\mathbf{Z}(\ell_i)^\top\}_{i=1}^{n_A})$  and  $\mathbf{D}_{\mathcal{A}} = \text{blockdiag}(\{\mathbf{D}\}_{i=1}^{n_A})$ . After fixing a reference set  $\mathcal{S}$ , we obtain  $\mathcal{S}^* = \mathcal{T} \cap \mathcal{S}$  and  $\mathcal{U} = \mathcal{T} \setminus \mathcal{S}$ . We partition the domain as above to obtain  $\mathcal{S}_j, \mathcal{S}_j^*, \mathcal{U}_j$  for  $j = 1, \dots, M$  and model  $\mathbf{w}(\ell)$  using the MGP which yields  $\mathbf{w} \sim N(\mathbf{0}, \widetilde{\mathbf{C}}_{\mathcal{S}}^{-1})$ . We complete the model specification by assigning  $\boldsymbol{\beta} \sim N(\boldsymbol{\beta} \mid \boldsymbol{\mu}_{\boldsymbol{\beta}}, \boldsymbol{\Sigma}_{\boldsymbol{\beta}})$ ,  $\tau_j^2 \sim \text{Inv.Gamma}(\tau_j^2 \mid a_{\tau_j}, b_{\tau_j})$ ,  $\boldsymbol{\theta} \sim p(\boldsymbol{\theta})$ .

The resulting full conditional distribution for  $\boldsymbol{\beta}$  is  $N(\boldsymbol{\Sigma}_{\boldsymbol{\beta}}^* \boldsymbol{\mu}_{\boldsymbol{\beta}}^*, \boldsymbol{\Sigma}_{\boldsymbol{\beta}}^*)$ , where  $\boldsymbol{\Sigma}_{\boldsymbol{\beta}}^* = (\boldsymbol{\Sigma}_{\boldsymbol{\beta}}^{-1} + \mathbf{X}^\top \mathbf{D}_n^{-1} \mathbf{X})^{-1}$ ,  $\boldsymbol{\mu}_{\boldsymbol{\beta}}^* = \boldsymbol{\Sigma}_{\boldsymbol{\beta}}^{-1} \boldsymbol{\mu}_{\boldsymbol{\beta}} + \mathbf{X}^\top \mathbf{D}_n^{-1} (\mathbf{y} - \mathbf{Z}\mathbf{w})$ . For  $\tau_r^2$ ,  $r = 1, \dots, q$ , the full conditional is Inverse-Gamma with parameters  $a_{\tau_r} + n/2$  and  $b_{\tau_r} + \frac{1}{2} \mathbf{E}_r^\top \mathbf{E}_r$  where  $\mathbf{E}_r = \mathbf{y}_{\cdot r} - \mathbf{X}_{\cdot r} \boldsymbol{\beta} - \mathbf{Z}_{\cdot r} \mathbf{w}$  and  $\mathbf{y}_{\cdot r}, \mathbf{X}_{\cdot r}, \mathbf{Z}_{\cdot r}$  are the subsets of  $\mathbf{y}, \mathbf{X}, \mathbf{Z}$  corresponding to the  $r$ th outcome (out of  $q$ ) of the multivariate output.

The Gibbs update of the  $\mathbf{w}_{\mathcal{U}}$  components can proceed simultaneously as all blocks in

$\mathcal{U}$  have no children and their parents are in  $\mathcal{S}$ . The full conditional for  $\mathbf{w}_{\mathcal{U}_j}$  for  $j = 1, \dots, M$  is thus  $N(\boldsymbol{\Sigma}_{\mathcal{U}_j}^* \boldsymbol{\mu}_{\mathcal{U}_j}^*, \boldsymbol{\Sigma}_{\mathcal{U}_j}^*)$  where  $\boldsymbol{\Sigma}_{\mathcal{U}_j}^* = (\mathbf{Z}(\mathcal{U}_j) \mathbf{D}^{-1} \mathbf{Z}(\mathcal{U}_j)^\top + \mathbf{R}_{\mathcal{U}_j}^{-1})^{-1}$  and  $\boldsymbol{\mu}_{\mathcal{U}_j}^* = \mathbf{Z}(\mathcal{U}_j) \mathbf{D}^{-1} (\mathbf{y}(\mathcal{U}_j) - \mathbf{X}(\mathcal{U}_j)^\top \boldsymbol{\beta}) + \mathbf{R}_{\mathcal{U}_j}^{-1} \mathbf{H}_{\mathcal{U}_j} \mathbf{w}_{[\mathbf{b}_j]}$ , where  $\mathbf{w}_{[\mathbf{b}_j]}$  is the spatial process at locations corresponding to the parents of  $\mathbf{b}_j \in \mathbf{B} \subset \mathbf{V}$ .

We update  $\mathbf{w}_{\mathcal{S}_j} = \mathbf{w}_j$  for  $j = 1, \dots, M$  via its full conditional  $N(\boldsymbol{\Sigma}_j^* \boldsymbol{\mu}_j^*, \boldsymbol{\Sigma}_j^*)$ . Let  $\mathbf{1}_j = (In(s_1 \in \mathcal{S}_j^*), \dots, In(s_{n_j} \in \mathcal{S}_j^*))^\top$  be the vector of indicators that identify locations with non-missing outputs, and let  $\mathbf{a}_j \in \mathbf{V}$  be the node in  $\mathcal{G}$  corresponding to  $\mathcal{S}_j$ . Then,

$$\begin{aligned} \boldsymbol{\Sigma}_j^{*-1} &= \mathbf{Z}_j^\top \tilde{\mathbf{D}}_{n_j}^{-1} \mathbf{Z}_j + \mathbf{R}_j^{-1} + \sum_{i=1}^{|\text{Ch}[\mathbf{a}_j]|} \mathbf{H}_i^{[j]\top} \mathbf{R}_i^{[j]-1} \mathbf{H}_i^{[j]} \\ \boldsymbol{\mu}_j^* &= \mathbf{R}_j^{-1} \mathbf{H}_j \mathbf{w}_{[j]} + \mathbf{Z}_j^\top \tilde{\mathbf{D}}_{n_j}^{-1} \tilde{\mathbf{y}}_j + \sum_{i=1}^{|\text{Ch}[\mathbf{a}_j]|} \mathbf{H}_i^{[j]\top} \mathbf{R}_i^{[j]-1} \mathbf{w}_i^{[j]}, \end{aligned} \quad (12)$$

where  $\tilde{\mathbf{D}}_{n_j}^{-1} = \mathbf{I}_j \odot \mathbf{D}_{n_j}^{-1}$  with  $\mathbf{I}_j = \mathbf{1}_j \mathbf{1}_j^\top$ , and  $\tilde{\mathbf{y}}_j = \mathbf{1}_j \odot (\mathbf{y}_j - \mathbf{X}_j \boldsymbol{\beta})$  and  $\odot$  denotes the Hadamard or Schur (element-by-element) product. Finally,  $\boldsymbol{\theta}$  is updated via a Metropolis step with target density  $p(\boldsymbol{\theta}) N(\mathbf{w}_{\mathcal{S}} \mid \mathbf{0}, \tilde{\mathbf{C}}_{\mathcal{S}}) N(\mathbf{w}_{\mathcal{U}} \mid \mathbf{H}_{\mathcal{U}} \mathbf{w}_{\mathcal{S}}, \mathbf{R}_{\mathcal{U}})$  using (8) and (10). The Gibbs sampling algorithm will iterate across the above steps and, upon convergence, will produce samples from  $p(\boldsymbol{\beta}, \{\tau_j^2\}_{j=1}^q, \mathbf{w} \mid \mathbf{y})$ .

We also use samples from this posterior distribution for prediction. For  $\ell \in \mathcal{D}$ , we obtain a sample of  $\mathbf{y}(\ell) \mid \mathbf{y}(\mathcal{T})$  as follows: if  $\ell \in \mathcal{S} \cup \mathcal{U}$  then  $\mathbf{y}(\ell) = \mathbf{X}(\ell)^\top \boldsymbol{\beta} + \mathbf{Z}(\ell)^\top \mathbf{w}(\ell)$ , where  $\boldsymbol{\beta}$  and  $\mathbf{w}$  are sampled from  $p(\boldsymbol{\beta}, \{\tau_j^2\}_{j=1}^q, \mathbf{w} \mid \mathbf{y})$ . Otherwise, considering that  $\ell \in \mathcal{D}_j$  for some  $j$  and thus  $\eta(\ell) = \mathbf{b}_j$ , with parent nodes  $\text{Pa}[\mathbf{b}_j]$  and children  $\text{Ch}[\mathbf{b}_j] = \emptyset$ , we sample  $\mathbf{w}(\ell)$  from the full conditional  $N(\boldsymbol{\Sigma}_\ell^* \boldsymbol{\mu}_\ell^*, \boldsymbol{\Sigma}_\ell^*)$  where  $\boldsymbol{\Sigma}_\ell^* = (\mathbf{Z}(\ell) \mathbf{D}^{-1} \mathbf{Z}(\ell)^\top + \mathbf{R}_\ell^{-1})^{-1}$  and  $\boldsymbol{\mu}_\ell^* = \mathbf{Z}(\ell) \mathbf{D}^{-1} (\mathbf{y}(\ell) - \mathbf{X}(\ell)^\top \boldsymbol{\beta}) + \mathbf{R}_\ell^{-1} \mathbf{H}_\ell \mathbf{w}_{[\mathbf{b}_j]}$ , then obtain  $\mathbf{y}(\ell) = \mathbf{X}(\ell)^\top \boldsymbol{\beta} + \mathbf{Z}(\ell)^\top \mathbf{w}(\ell)$ .

### 3.2 Computations with non-separable multivariate space-time base covariances

We provide an account of the computational cost of general MGPs as a starting point to motivate the introduction of more efficient tessellated MGPs, and specifically Q-MGPs, in Section 4. We consider (11) and take  $l = 1$  to simplify our exposition. In the resulting univariate regression,  $\boldsymbol{\beta}$  is the usual linear regression coefficient on the  $p$  point-referenced regressors assumed to have a constant effect on the outcome, whereas the  $q$ -variate spa-

tiotemporal process  $\mathbf{w}(\cdot)$  captures the variable effect of the  $\mathbf{Z}$  regressors on the outcome. If  $p$  and  $q$  are small, as is the case in typical geostatistical modeling, sampling  $\boldsymbol{\beta}$  and  $\tau^2$  carries a negligible computational cost. The cost of each Gibbs iteration is dominated by updates of  $\boldsymbol{\theta}$  and  $\mathbf{w}$ . Let us assume, solely for expository purposes, that each of the  $M$  blocks comprise the same number of locations, i.e.  $|\mathcal{S}_j| = |\mathcal{U}_j| = m$ , for all  $j = 1, \dots, M$ . Thus,  $m = \frac{n}{2M}$  and the graph nodes have  $J$  or fewer parents and  $L$  or fewer children.

The evaluation of  $N(\mathbf{w}_S | \mathbf{0}, \tilde{\mathbf{C}}_S) = \prod_{j=1}^M N(\mathbf{w}_j | \mathbf{H}_j \mathbf{w}_{[j]}, \mathbf{R}_j)$  and  $N(\mathbf{w}_U | \mathbf{H}_U \mathbf{w}_S, \mathbf{R}_U) = \prod_{j=1}^M N(\mathbf{w}_{U_j} | \mathbf{H}_{U_j} \mathbf{w}_{[b_j]}, \mathbf{R}_{U_j})$  dominates the overall computational expense. Each term in the product requires computing  $\mathbf{R}_j^{-1}$  and  $\mathbf{R}_{U_j}^{-1}$ , both of size  $qm \times qm$ , and their determinant. These, in turn, require  $\mathbf{C}_{[j],[j]}^{-1}$  of size  $Jqm \times Jqm$  or less, resulting in  $O(2M(q^3m^3 + J^3q^3m^3)) = O(2Mq^3m^3(J^3 + 1)) \approx O(2Mq^3m^3J^3) = O(\frac{n^3q^3J^3}{M^2})$  flops via Cholesky decompositions. Reasonably,  $J$  and  $m$  are fixed so  $M$  may grow linearly with sample size, so the cost is  $O(nq^3J^3)$  considering  $M \propto n$ . The total computing time is approximately  $O(\frac{nq^3J^3}{K})$  when using  $K$  processors to compute the  $2M$  densities.

Sampling  $\mathbf{w}_S$  and  $\mathbf{w}_U$  from their full conditional distributions requires  $O(2Mq^3m^3 + MLq^2m^2 + Mq^2m^2)$  flops, assuming  $\mathbf{R}_j^{-1}$  and  $\mathbf{R}_{U_j}^{-1}$  have been stored in the previous step. The first term in the complexity order is due to the Cholesky decomposition of covariance matrices in the full conditionals, the second to sampling the reference nodes, and the third is due to sampling other nodes. Without additional assumptions, parallelization brings the time down to  $O(\frac{2Mq^3m^3}{K} + \frac{Mq^2m^2}{K} + MLq^2m^2)$ , since the covariances can be computed beforehand and the  $M$  components of  $\mathbf{w}_U$  are independent given  $\mathbf{w}_S$ . With fixed block size  $m$ , the overall time for a Gibbs iteration is thus  $O(\frac{2}{K}Mq^3m^3(J^3 + 1) + \frac{1}{K}2Mq^3m^3 + \frac{1}{K}Mq^2m^2 + MLq^2m^2) \approx O(\frac{1}{K}J^3q^3n + q^2n) \approx O(n)$ , linear in the sample size and cubic in  $J$ , highlighting the computational speedup of sparse graphs ( $J$  small), the negative impact of large  $q$ , and the serial sampling of  $\mathbf{w}_S$ .

In terms of storage, no large matrices (dense or sparse) need to be computed and/or stored. The  $\mathbf{H}_j$  and  $\mathbf{R}_j$  matrices correspond to a storage requirement  $O(4Mq^2m^2) = O(q^2n)$ . The matrix  $\mathbf{Z}$  of size  $qn \times qn$  will never be computed. Instead, it can be represented as a list of  $2M$  block-diagonal (thus sparse)  $\mathbf{Z}_j$  matrices. Furthermore, computing  $\mathbf{Z}\mathbf{w}$  (dimension  $n \times 1$ ) can be vectorized as the row-wise sum of  $\mathbf{Z}^* \odot \mathbf{w}^*$  where  $\mathbf{Z}^*$  and  $\mathbf{w}^*$  are  $n \times q$  matrices whose  $j$ th column represents the  $j$ th space-time varying predictor. Storing  $\mathbf{Z}$  both as a list

and as  $\mathbf{Z}^*$  results in total storage of  $O(2qn)$ .

Complexity is further reduced by considering a graph with small  $J$  or a finer partition resulting in large  $M$  and small  $m$ , whereas the overall time can be reduced by distributing computations on  $K$  processors. Possible choices for  $\mathcal{G}$  include nearest-neighbor graphs and multiresolution trees. The former considers very fine domain partitioning ( $M \approx n$  and  $m = 1$ ) and restricts graph connectedness by limiting the number of neighbors (i.e. parents) typically to  $J < 20$ . Serial updates of  $\mathbf{w}_{\mathcal{S}}$  will be prone to slow mixing when spatial correlation is high, Sparse Cholesky methods for block updates depend on the precision matrix fill-in (Yannakakis, 1981) and are generally much more expensive. A multiresolution tree associated with domain partitioning in  $J + 1$  recursive steps results in “last-generation” children (leaves) with  $J$  parents.  $J$  may grow sublinearly with sample size, but  $m$  will have to be very small to avoid excessive slow-downs. In settings with large  $q$ , adjusting  $J$  and  $M$  may insufficiently reduce the computational burden. In such cases, at the cost of flexibility and model richness one may opt for a cross-covariance function that is separable in the variables (but perhaps non-separable in space and time), bringing the cost of inversion of  $Jqm \times Jqm$  matrices from  $O(J^3q^3m^3)$  to  $O(J^3m^3 + q^3)$  since in that case  $\mathbf{C}^{-1} = (\mathbf{C}_{\mathbf{h},u} \otimes \mathbf{C}_{\mathbf{v}})^{-1} = \mathbf{C}_{\mathbf{h},u}^{-1} \otimes \mathbf{C}_{\mathbf{v}}^{-1}$ , where  $\mathbf{C}_{\mathbf{h},u}$  is the  $Jm \times Jm$  space-time component of the cross-covariance, and  $\mathbf{C}_{\mathbf{v}}$  the  $q \times q$  variable component. This also applies to any Cholesky decomposition, so there will be savings when evaluating the likelihood as well as in sampling from the full-conditionals.

As a cheaper alternative, we develop algorithms based on domain tessellation – i.e. partitioning on regions shaped similarly to form patterns – to which we associate similarly patterned meshes. With irregularly spaced observations, a the bulk of the largest linear solvers will be redundant, resulting in a significant reduction in computational time. These redundancies are larger if data are on partly observed regular lattices. In either scenario, sampling  $\mathbf{w}_{\mathcal{S}}$  will also proceed in parallel with improved mixing.

## 4 MGPs based on domain tessellation or tiling

We partition the domain using a tessellation or tiling. For spatial domains ( $d = 2$ , Figure 2), regular tiling results in triangular, quadratic, or hexagonal tessellations, but mixed designs are also possible. These partition schemes can be linked to a DAG  $\mathcal{G}$  by drawing directed

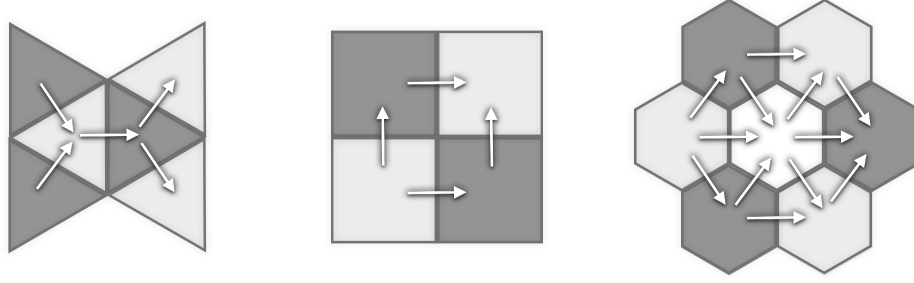


Figure 2: Regular tessellation base units and corresponding MGP graphs for spatial domains.

outgoing edges starting from an originating node/tile. The same fixed pattern can be repeated over a surface of any size. In dimensions  $d > 2$ , which may include time, space-filling tessellations or honeycombs can be constructed analogously, along with their corresponding meshes. Constructing MGPs based on these tessellation and graph designs is immediate and simply requires partitioning the locations  $\mathcal{S}$  and  $\mathcal{U}$  into subsets based on the chosen tessellation.

This subclass of MGP models enjoys two properties. First, each node in  $\mathcal{G}$  can be linked to a color; if node  $\mathbf{v}$  is colored  $c$  and we remove from  $\mathcal{G}$  all nodes of other colors,  $\mathbf{v}$  will be disconnected from all other nodes of the same color in the moral graph  $\mathcal{G}^{\mathcal{M}}$ . This means that the graph itself can be partitioned into conditionally independent subgraphs, one for each color. The number of colors is small, e.g. 3, 4, 6 for triangles, squares, and hexagons, respectively. This enables large-scale parallel sampling of  $\mathbf{w}_{\mathcal{S}}$  and improves mixing. Second, each region in the tessellated domain is a translation and/or rotation of a single geometric shape; it is linked to nodes in  $\mathcal{G}$  with a fixed number of parents and children, and the parent regions are also the translation and/or rotation of the same geometric shapes. Carefully choosing  $\mathcal{S}$ , it will be possible to avoid computing the bulk of linear solvers, resulting in substantial computational gains. Subsequently, we focus on axis-parallel partitioning (quadratic or cubic tessellation) and cubic meshes, but analogous constructions and the same properties hold with other tessellation schemes.

A cubic MGP (Q-MGP) can be constructed by partitioning each coordinate axis into intervals. In  $d + 1$  dimensions, splitting each axis into  $L$  intervals results in  $L^{d+1}$  regions. Consider a spatiotemporal domain  $\mathcal{D} = \times_{r=1}^{d+1} \mathcal{D}^{(r)}$ , where  $\mathcal{D}^{(d+1)}$  is the time dimension. We partition each coordinate axis into  $L_r$  disjoint sets:  $\mathcal{D}^{(r)} = \mathcal{I}_{r,1} \cup \dots \cup \mathcal{I}_{r,L_r}$ , where



$\mathcal{I}_{r,j} \cap \mathcal{I}_{r,k} = \emptyset$  if  $j \neq k$  and  $\mathcal{I}_{r,s}$  denotes the  $s$ th interval in the  $r$ th coordinate axis. Solely for exposition and without loss of generality, assume that  $\mathcal{D}^{(r)} = \mathcal{I} = [0, 1]$  and  $L_r = L$  for  $r = 1, \dots, d+1$  to simplify exposition. Any location  $\ell = (\ell_1, \dots, \ell_{d+1}) \in \mathcal{D}$  will be such that  $\ell \in \mathcal{I}_{1,i_1} \times \dots \times \mathcal{I}_{d+1,i_{d+1}} = \mathcal{D}_j$  for some  $i_1, \dots, i_{d+1}$  and with  $j = 1, \dots, M$ , where  $M = L^{d+1}$ . We refer to this axis-parallel partition scheme as a cubic tessellation and denote it by  $\mathbf{T} = \{\mathcal{I}_{r,s}\}_{r=1,\dots,d+1}^{s=1,\dots,L}$ . We use  $\mathbf{T}$  to partition the reference set  $\mathcal{S}$  as  $\mathcal{S}_j = \mathcal{D}_j \cap \mathcal{S}$  for  $j = 1, \dots, L^{d+1}$ .

Next, we define  $\eta(\ell) = (\eta_1(\ell), \dots, \eta_L(\ell)) \in \{1, \dots, L\}^{d+1}$ , where  $\eta_j = \eta_j(\ell) = r$  if  $\ell_j \in \mathcal{I}_{j,r}$ . Then, let  $\mathcal{Q} = (\mathbf{V}, \mathbf{E})$  be a directed acyclic graph with  $\mathbf{V} = \mathbf{A} \cup \mathbf{B}$  and reference nodes  $\mathbf{A} = \{\mathbf{a}_1, \dots, \mathbf{a}_{L^{d+1}}\}$ . Therefore, for any  $j = 1, \dots, L^{d+1}$  if  $\mathbf{s} \in \mathcal{S}_j$  then  $\eta(\mathbf{s}) = \mathbf{a}_j \in \mathbf{A} \subset \mathbf{V}$ . We write each node  $\mathbf{v} \in \mathbf{V}$  as  $\mathbf{v} = (v_{\eta_1}, \dots, v_{\eta_L}) \in \{1, \dots, L\}^{d+1}$ . The directed edges are constructed using a “line-of-sight” strategy. Suppose  $\text{Pa}[\mathbf{v}] = \{\mathbf{x}^{(1)}, \dots, \mathbf{x}^{(d+1)}\}$ . The  $h$ th parent of  $\mathbf{v}$  is defined as  $\mathbf{x}^{(h)} = (a_{\eta_1}, \dots, a_{\eta_h} - k, \dots, a_{\eta_L}) \cap \{1, \dots, d+1\}^{d+1}$ , where  $k \geq 1$  is the smallest integer such that  $\mathbf{x}^{(h)} \in \mathbf{A}$ . Consequently  $\mathbf{x}^{(h)} = \emptyset$  if  $a_h = 1$ . Thus, the parents of node  $\mathbf{v} = \eta(\ell)$  are the ones that precede it along each of the  $d+1$  coordinates. If  $\ell \in \mathcal{D}_j \setminus \mathcal{S}_j$ , then  $\eta(\ell) = \mathbf{b}_j \in \mathbf{B}$  and  $\text{Pa}[\mathbf{b}_j] = \{\mathbf{a}_j\} \cup \text{Pa}[\mathbf{a}_j]$  where  $\mathbf{a}_j \in \mathbf{A}$  is a reference node. This scheme is incomplete if there is  $\mathcal{D}_j$  such that  $\mathcal{S}_j = \emptyset$ , which may arise if large parts of the spatial domain are not observed and  $\mathcal{S}$  is not chosen to cover the whole domain. To avoid having  $\text{Pa}[\mathbf{b}_j] = \emptyset$ , one may set  $\text{Pa}[\mathbf{b}_j] = \{\mathbf{x}_1^{(1)}, \mathbf{x}_2^{(1)}, \dots, \mathbf{x}_1^{(d+1)}, \mathbf{x}_2^{(d+1)}\}$ . The two parents along the  $h$ th dimension are  $\mathbf{x}_1^{(h)} = a_{\eta_h} + k_1$ ,  $\mathbf{x}_2^{(h)} = a_{\eta_h} - k_2$  where  $k_i$  is the smallest positive integer such that  $\mathbf{x}_i^{(h)} \in \mathbf{A}$ ,  $i = 1, 2$ . In other words, these locations have parents along all  $2(d+1)$  line-of-sight directions. This scenario corresponds to  $J = 2(d+1)$  and can be avoided by choosing  $\mathcal{S}$  to cover the observed locations, in which case  $J = d+2$ .

The construction is finalized by fixing the cross-covariance function  $\mathbf{C}(\ell, \ell')$ , resulting in a  $\text{MGP}(\mathcal{Q}, \mathbf{T}, \mathcal{S}, \mathbf{C}) = \text{Q-MGP}(\mathcal{S}, \mathbf{C})$ . Figure 3 how the same basic structure can be immediately extended to higher dimensions, including time.

## 4.1 Caching redundant expensive matrix operations

The key computational bottleneck of the Gibbs sampler in Section 3.2 is the calculation for  $j = 1, \dots, 2M$  of (1)  $\mathbf{C}_{[j],[j]}^{-1}$  ( $2MJ^3q^3m^3$  flops) and (2)  $\mathbf{R}_j^{-1}$ ,  $\Sigma_j^{*-1}$  ( $4Mq^3m^3$  flops). The former is costlier than the latter by a factor of  $J^3/2$ . Q-MGPs can be designed to greatly

reduce this cost. Start with an axis-parallel tessellation of the domain in equally-sized regions  $\mathcal{D}_1, \dots, \mathcal{D}_M$ , storing observed locations in  $\mathcal{U}$  to create  $\mathcal{U}_1, \dots, \mathcal{U}_M$ , which we assume for simplicity to be no larger than  $m$  in size. Take a stationary base-covariance function  $\mathbf{C}$ . For any two sets of locations,  $\mathcal{L}_1$  and  $\mathcal{L}_2$ , this implies that  $\mathbf{C}(\mathcal{L}_1, \mathcal{L}_2) = \mathbf{C}(\mathcal{L}_1 + \mathbf{h}, \mathcal{L}_2 + \mathbf{h})$ , where  $\mathbf{h} \in \mathbb{R}^{d+1}$  is used to shift all locations in the sets. Recall that the knot set or reference set  $\mathcal{S}$  of MGPs can include unobserved locations. With this in mind, we can build  $\mathcal{S}$  on a lattice of regularly spaced locations. Since all domain partitions have the same size,  $\mathcal{S}_j = \mathcal{S}^* + \mathbf{h}_j$  for  $j = 1, \dots, M$ , where  $\mathcal{S}^*$  is a single “prototype set” using which one can locate all other reference subsets. Similarly, considering that  $\text{Pa}[\mathbf{a}_j] \subset \text{Pa}[\mathbf{b}_j]$ , there will be  $4(d+1)$  prototype sets for parents, i.e.  $\mathcal{S}_{\text{Pa}[\mathbf{v}_j]} = \mathcal{S}_r^* + \mathbf{h}_j$  for some  $r \in \{1, \dots, 4(d+1)\}$  and  $j = 1, \dots, 2M$ . Then, we can build maps  $\xi_{\mathcal{S}} : \{1, \dots, M\} \rightarrow \{1, \dots, 4(d+1)\}$  and  $\xi_{\mathcal{U}} : \{1, \dots, M\} \rightarrow \{1, \dots, 4(d+1)\}$  linking each of  $\mathcal{S}_j$  and  $\mathcal{U}_j$  to a parent prototype. Then, for all  $j = 1, \dots, 2M$ , there exists  $r$  such that  $\mathbf{C}_{[j],[j]}^{-1} = \mathbf{C}_{\mathcal{S}_r^*, \mathcal{S}_r^*}^{-1}$ . In other words one only needs to create the maps  $\xi_{\mathcal{S}}$  and  $\xi_{\mathcal{U}}$ , *cache* the  $r$  unique inverses, and reuse them to avoid recalculating the inverses. We can use the same method to cache  $\mathbf{R}_{\mathcal{S}_j}^{-1} = \mathbf{R}_{\mathcal{S}_r^*}^{-1}$  on reference sets, but not on other locations since no redundancy arises in  $\mathbf{C}_{\mathcal{U}_j, \mathcal{U}_j}$  for  $j = 1, \dots, M$ , making  $\mathbf{R}_{\mathcal{U}_j}^{-1}$  all different in general. Compared to general MGPs (see Table 1), the number of large linear system solvers is now constant with sample size; notice that  $(d+1) \ll M$  implies in a large reduction in computational cost.

Furthermore, Q-MGPs can automatically adjust to settings where observed locations  $\mathcal{T}$  are on partly regular lattices meaning that they are located at patterns which repeat in space and time. These patterns emerge after initial inspections of the data. We outline a simple algorithm to identify simple patterns and create maps  $\xi_{\mathcal{S}}$  and  $\xi_{\mathcal{U}}$  in Appendix E. In those cases, we fix  $\mathcal{S} \supseteq \mathcal{T}$  and  $\mathcal{U} = \emptyset$ . In addition to the above mentioned savings, we now do not have to compute  $\mathbf{R}_{\mathcal{U}_j}^{-1}$  and  $\Sigma_{\mathcal{U}_j}^{*-1}$ . If  $\mathcal{T}$  are not on a regular lattice over the whole domain, the  $4(d+1)$  is a lower bound and in general there will be  $M^* \ll M$  inverses to compute. The very special case in which  $\mathcal{T}$  is itself a fully observed regular lattice and if  $\mathbf{Z}(\ell) = I$  (spatially varying intercept model), then one can expect savings in computing the full conditional covariances as well, since all  $\mathbf{D}_j = I$ . Refer to Appendix B.1 for additional considerations on the choice of  $\mathcal{S}$  and  $\mathcal{U}$ .

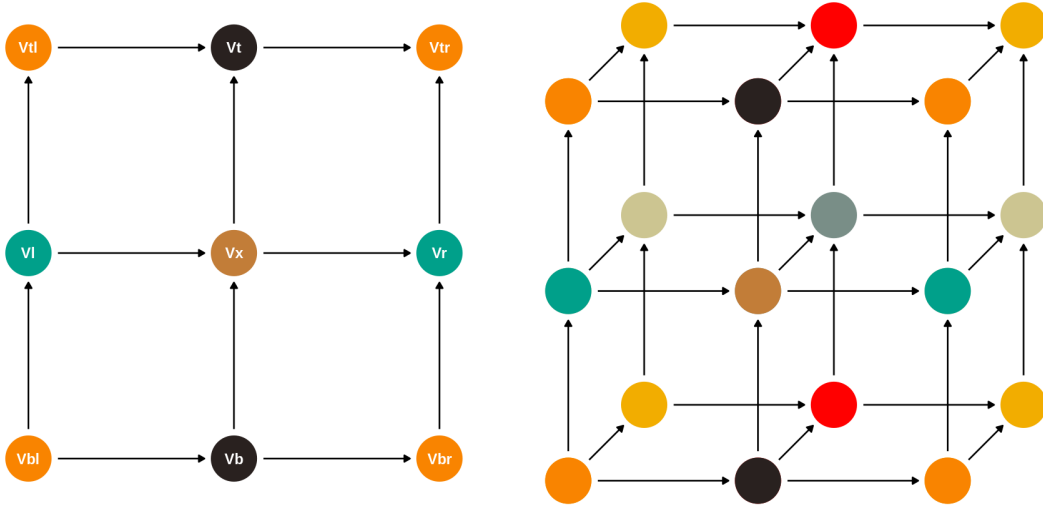


Figure 3: Q-MGP meshes used for spatial data on  $d = 2$  (left) can be extended for use on spatiotemporal data  $d = 3$  (right). Node colors correspond to Gibbs sampler blocks.

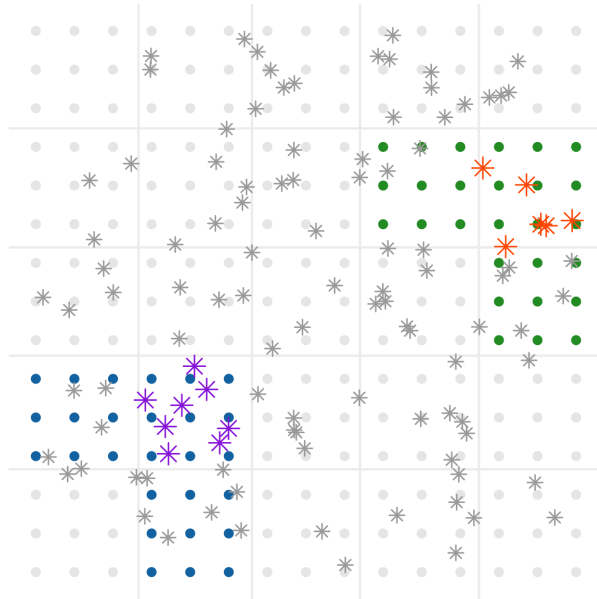


Figure 4: Visualizing redundancies: a spatial domain is partitioned in  $M = 25$  regions and linked to a quadratic mesh. The reference set  $\mathcal{S}$  is fixed on a regular grid, with  $m = 9$ . Parent locations of the orange (resp. purple) are in green (resp. blue). Using a stationary covariance,  $\mathbf{C}_{\text{blue,blue}} = \mathbf{C}_{\text{green,green}}$ . Therefore only one inversion is necessary; this can be replicated at no cost across 9 of the 16 regions.

	$C_{[j],[j]}^{-1}$	$R_{S_j}^{-1}$	$R_{u_j}^{-1}$	$\Sigma_{S_j}^{*-1}$	$\Sigma_{u_j}^{*-1}$	Sampling $\mathbf{w}_S, \mathbf{w}_U$
MGPs (all cases)	$2MJ^3q^3m^3$	$Mq^3m^3$	$Mq^3m^3$	$Mq^3m^3$	$Mq^3m^3$	$MLq^2m^2 + Mq^2m^2$
<i>Q-MGPs</i>						
— Irregular locations	$4(d+1)J^3q^3m^3$	$4(d+1)q^3m^3$	$Mq^3m^3$	$Mq^3m^3$	$Mq^3m^3$	$MLq^2m^2 + Mq^2m^2$
— Pattern lattice w/missing	$2M^*J^3q^3m^3$	$2M^*q^3m^3$		$Mq^3m^3$		$MLq^2m^2$
— Lattice w/ missing	$4(d+1)J^3q^3m^3$	$4(d+1)q^3m^3$		$Mq^3m^3$		$MLq^2m^2$
— Full lattice and $\mathbf{Z}(\ell) = I_q$	$4(d+1)J^3q^3m^3$	$4(d+1)q^3m^3$		$2^{(d+2)}(d+1)q^3m^3$		$MLq^2m^2$

Table 1: Summary of computational cost of general MGPs and Q-MGPs. All operations can be performed in parallel except those in red. Rows are sorted from most expensive (top) to least expensive (bottom).

## 4.2 Improved mixing via parallel sampling

Caching in Q-MGPs greatly reduces computing cost and time, therefore a much larger proportion of time is spent on sampling. Fortunately, MGPs on tessellated domains such as Q-MGPs are associated with efficient parallel sampling of the latent spatial random effects via a “chromatic” sampler (Gonzalez et al., 2011). Reference nodes  $\mathbf{A}$  of  $\mathcal{Q}$  are partitioned into groups or colors, and nodes of the same color are conditionally independent given realizations of reference nodes of other colors. To see this, we partition a spatial domain ( $d = 2$ ) into  $M_1 \times M_2$  regions and link each region to a reference node in a quadratic mesh. We define a “central” reference node as one that has two parents and two children, i.e. if  $\mathbf{v}_+$  is central then  $\text{Pa}[\mathbf{v}_+] = \{\mathbf{v}_l, \mathbf{v}_b\}$  and  $\text{Ch}[\mathbf{v}_+] = \{\mathbf{v}_r, \mathbf{v}_t\}$ , with  $l, b, r, t$  respectively denoting *left, bottom, right, top*. Figure 3 (left) depicts a central node and its neighbors. We have  $\text{Pa}[\mathbf{v}_t] = \{\mathbf{v}_+, \mathbf{v}_{tl}\}$  and  $\text{Pa}[\mathbf{v}_r] = \{\mathbf{v}_+, \mathbf{v}_{br}\}$ . The Markov blanket of  $\mathbf{v}_+$ , denoted as  $\text{mb}(\mathbf{v}_+)$ , is the set of neighbors of  $\mathbf{v}_+$  in the undirected “moralized” graph  $\mathcal{Q}^M$ , hence  $\text{mb}(\mathbf{v}_+) = \text{Pa}[\mathbf{v}_+] \cup \text{Ch}[\mathbf{v}_+] \cup \{\mathbf{v}_{tl}, \mathbf{v}_{br}\}$ . The corresponding spatial process will then be such that  $p(\mathbf{w}_+ \mid \mathbf{w} \setminus \mathbf{w}_+) = p(\mathbf{w}_+ \mid \mathbf{w}_{\text{mb}(\mathbf{v}_+)})$ . Denoting  $\mathbf{v}_{bl} = \text{Pa}[\mathbf{v}_l] \cap \text{Pa}[\mathbf{v}_b]$  and  $\mathbf{v}_{tr} = \text{Ch}[\mathbf{v}_r] \cap \text{Ch}[\mathbf{v}_t]$ , we note that  $\{\mathbf{v}_{bl}, \mathbf{v}_{tr}\} \cap \text{mb}(\mathbf{v}_+) = \emptyset$ . We partition reference nodes  $\mathbf{A}$  into four groups  $\{\mathbf{A}^{(1)}, \mathbf{A}^{(2)}, \mathbf{A}^{(3)}, \mathbf{A}^{(4)}\}$ , such that  $\{\mathbf{v}_+\} \subset \mathbf{A}^{(1)}$ ,  $\{\mathbf{v}_b, \mathbf{v}_t\} \subset \mathbf{A}^{(2)}$ ,  $\{\mathbf{v}_l, \mathbf{v}_r\} \subset \mathbf{A}^{(3)}$ , and  $\{\mathbf{v}_{tl}, \mathbf{v}_{tr}, \mathbf{v}_{bl}, \mathbf{v}_{br}\} \subset \mathbf{A}^{(4)}$ . This  $3 \times 3$  pattern is repeated over the whole graph. Then, if  $\mathbf{v} \in \mathbf{A}^{(j)}$ ,  $\text{mb}(\mathbf{v}) \cap \mathbf{A}^{(j)} = \emptyset$ . Denoting by  $\mathcal{D}$  the other conditioning variables

in the Gibbs sampler, we obtain

$$p(\mathbf{w}_j \mid \mathbf{w}_{-j}, \mathcal{D}) = p(\mathbf{w}_j \mid \mathbf{w}_{\text{mb}(\mathbf{v}_j)}, \mathcal{D}) = \prod_{\mathbf{v}_i \in \mathbf{A}^{(j)}} p(\mathbf{w}_i \mid \mathbf{w}_{\mathbf{A}^{(-j)}}, \mathcal{D}).$$

Analogous results can be obtained for other tessellation schemes. Extensions to higher dimensions or space-time domains and the associated graphs also follow analogously.

Since parallelization is possible within each of the four groups, there will only be four serial steps. Compute times are now improved, given that  $M/4$  is typically several orders of magnitude larger than the number of available processors  $K$ . In addition to faster computations, this four-group design improves mixing of the Markov chain. We compare Q-MGPs with sequential NNGPs in terms of effective sample size in Appendix [F.2](#).

## 5 Data analysis

Satellite imaging and remote sensing data are nowadays frequently collected in large quantities and processed to be used in geology, ecology, forestry, and other fields. Unfortunately, cloud cover and atmospheric conditions obstruct aerial views and corrupt the data creating gaps. Recovery of the underlying signal, reconstruction of the missing areas in the images, and quantification of prediction uncertainty are thus the major goals to enable practitioners in the natural sciences to fully exploit these data sources. Geostatistical models based on Gaussian Processes deal with these issues rigorously, but many of the recently developed scalable models have only been implemented on tens or hundreds of thousands of data points, with few exceptions. In considering larger data sizes, one must either have a large time budget – usually several days – or reduce model flexibility and richness. Scalability concerns become the single most important issue in multivariate spatiotemporal settings. In fact, repeated collection of aerial images and multiple spatially-referenced predictors modeled to have a variable effect on the outcome have a multiplicative effect on data size. With no separability assumptions, the dimension of the latent spatial random effects that one may wish to recover will be huge even when individual images would be manageable when considered individually.

There is currently a lack of software to implement scalable models for spatial data that can be extended to spatiotemporal settings, making it difficult to compare our proposed ap-

proach with others in these settings. On the other hand, a recent competition paper (Heaton et al., 2019) has pinned many state-of-the-art models against each other in a spatial ( $d = 2$ ) prediction contest. In order to provide comparisons with those models, we analyze the same data in Appendix D, where we show that Q-MGPs can be set up to outperform all competitors in terms of predictive performance and coverage when using a similar computational budget.

## 5.1 Non-separable multivariate spatiotemporal base covariance

In our analyses, we choose a class of multivariate space-time cross-covariances that models the covariance between variables  $i$  and  $j$  at the  $(\mathbf{h}, u) \in \mathbb{R}^{d+1}$  space-time lags as:

$$\mathbf{C}_{ij}(\mathbf{h}, u) = \frac{\sigma^2}{\left(\psi_1\left(\frac{|u|^2}{\psi_2(\delta_{ij}^2)}\right)\right)^{d/2} (\psi_2(\delta_{ij}^2))^{1/2}} \phi_1\left(\frac{\|\mathbf{h}\|^2}{\psi_1\left(\frac{|u|^2}{\psi_2(\delta_{ij}^2)}\right)}\right), \quad (13)$$

where  $\delta_{ij} > 0$  (and with  $\delta_{ij} = \delta_{ji}$ ) is the latent dissimilarity between variables  $i$  and  $j$ . In the resulting cross-covariance function  $\mathbf{C}(\mathbf{h}, u, \mathbf{v})$  in  $\mathbb{R}^{d+1+k}$ , each component of the  $q$ -variate spatial process is represented by a point in a  $k$ -dimensional latent space,  $k \leq q$ . This multivariate cross-covariance function was introduced by Apanasovich and Genton (2010) as a generalization of the space-time covariance functions of Gneiting (2002) for  $q > 1$ . We choose  $\phi_1(x) = \exp(-cx)$  and  $\psi_j(x) = (a_j x^{\alpha_j} + 1)^{\beta_j}$ ,  $j = 1, 2$ ; refer to Gneiting (2002) for alternatives. In all applications, we fix  $\alpha_1 = \alpha_2 = \frac{1}{2}$ , and seek to estimate  $\boldsymbol{\theta} = (\sigma^2, c, a_1, \beta_1, a_2, \beta_2, \{\delta_{ij}\}_{i < j, j=1, \dots, q})$  a posteriori. Notice that the usual exponential covariance arises in univariate spatial settings.

## 5.2 Synthetic data

We aim to test the predictive ability of Q-MGP models in controlled settings that mimic real world satellite imaging data analyzed later in Section 5.3, but at a much smaller scale. We generate 81 synthetic spatiotemporal univariate datasets from the model  $\mathbf{y}(\boldsymbol{\ell}) = \mathbf{Z}(\boldsymbol{\ell})^\top \mathbf{w}(\boldsymbol{\ell}) + \boldsymbol{\varepsilon}(\boldsymbol{\ell})$ , where  $\boldsymbol{\varepsilon}(\boldsymbol{\ell}) \sim N(0, \tau^2)$  with  $\boldsymbol{\ell} \in \mathcal{T}$  and  $\mathcal{T}$  is a regular grid of size  $40 \times 40 \times 10$ . This results in  $n_{\text{all}} = 16,000$  total locations. We take  $\mathbf{w} \sim GP(\mathbf{0}, \mathbf{C})$  where  $\mathbf{C}$  is as in eq. (13) taking  $\psi_2 \equiv 1$  and  $\sigma^2 = 1$ . We generate one dataset for each combination

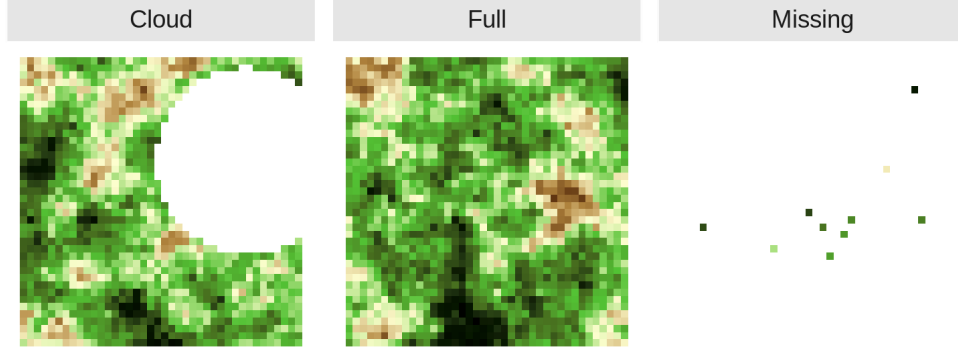


Figure 5: Artificial cloud covering in synthetic data.

of parameter choices  $\tau^2 \in \{1/1000, 1/20, 1/10\}$ , temporal range  $\alpha \in \{5, 50, 500\}$ , space-time separability  $\beta \in \{1/20, 1/2, 1 - \frac{1}{20}\}$ , and spatial range  $c \in \{1, 5, 25\}$ .

Our goal is to compare Q-MGPs with the specialized Gapfill method of [Gerber et al. \(2018\)](#), which was created to recover satellite imaging data when obstructed by clouds. We create “synthetic clouds” of radius  $\sqrt{0.1}$  and with center  $(c_{1,t}, c_{2,t}) \in [0, 1/20]^2$  where  $c_{1,t}, c_{2,t} \stackrel{iid}{\sim} U[0, 1]$  to cover the outcomes at six randomly selected times for each of the 81 datasets. Outcomes at two of the remaining four time periods were then randomly selected to be completely unobserved, save for 10 locations (this was necessary to avoid fitting errors for Gapfill). Figure 5 depicts the three cloud cover types.

We implemented a Q-MGP model with  $M = 500$  found by partitioning each spatial axis into 10 intervals, and the time axis into 5 intervals. We assigned priors  $\tau^2 \sim \text{Inv.G.}(2, 1)$ ,  $\sigma^2 \sim \text{Inv.G.}(2, 1)$ ,  $\beta \sim U(0, 1)$ ,  $\alpha \sim U(0, 10^4)$ ,  $c \sim U(0, 10^4)$  and run a Gibbs sampler for a total of 7000 iterations, of which 5000 used for burn-in and thinning the remaining 2000 to obtain an approximate posterior sample of size 1000.

For each of the 81 datasets and for both methods, we calculate the mean absolute prediction error (MAE) and the root mean squared prediction error (RMSE). We compare Gapfill’s approximated 90% intervals with 90% posterior equal-tailed credible intervals for the Q-MGP predictions as obtained from 1000 posterior samples of MCMC. In terms of MAE the Q-MGP model outperformed Gapfill in all datasets; in terms of RMSE, it outperformed Gapfill in 80 of 81 datasets. The average MAE of Q-MGP was 0.4094 against Gapfill’s 0.5366; the average RMSE was 0.5308 against Gapfill’s 0.6820. The Q-MGP model also resulted in much better



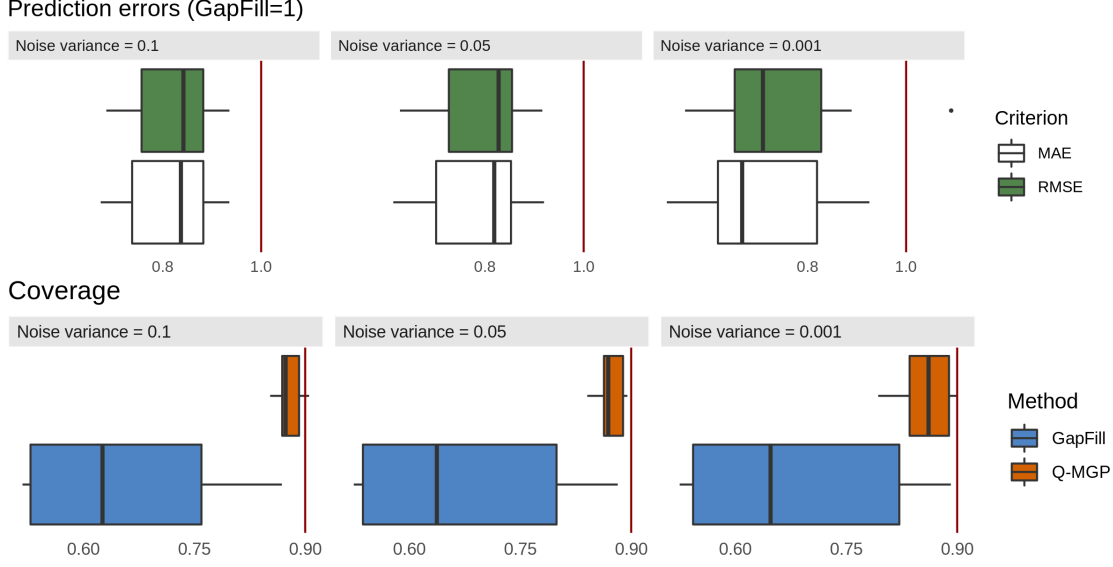


Figure 6: Performance of Q-MGP and Gapfill in out-of-sample predictions in 81 spatiotemporal datasets, at the three tested levels of noise variance  $\tau^2$ .

coverage of the prediction intervals, although some under-coverage was observed. Figure 6 summarizes these findings. We note that this comparison may favor our Q-MGP model since it directly approximates the true Gaussian process generating the data. For this reason, we consider the problem of recovering missing pixels of an animated GIF image in Appendix G; our findings are confirmed.

### 5.3 NDVI data from the Serengeti ecosystem

Time series of Normalized Difference Vegetation Index (NDVI) derived from satellite imagery are used to understand spatial patterns in vegetation phenology. For such studies, image pixel-level NDVI values are observed over time to assess seasonal trends in vegetation green-up, growing season length and peak, and senescence. These analyses typically require NDVI values for all pixels over the region and time period of interest. As noted in the beginning of this section, atmospheric conditions, e.g., cloud cover, and sensor malfunction cause missing NDVI pixel values and hence predicting such values, i.e., gap-filling, is of key interest to the remote sensing community. Here, we consider NDVI data derived from the LandSat 8 sensor (which provides a  $\sim 30 \times 30$  m spatial resolution pixel) taken over Serengeti National Park, Tanzania, Africa. These data were part of a larger study conducted by [Desanker et al.](#)

(2019) that looked at environmental drivers in vegetation phenology change. The data cover an area of  $30 \times 30$  km and 34 months, and correspond to 64 images of size  $1000 \times 1000$  collected at 16-day intervals. Data on NDVI are complemented with elevation and soil moisture data, for a total of three spatially referenced predictors. We are thus interested in understanding their varying effect in space and time, in addition to predicting NDVI output at missing locations. We achieve both these goals by implementing the model

$$\mathbf{y}(\ell) = \mathbf{X}(\ell)\boldsymbol{\beta} + \mathbf{Z}(\ell)\mathbf{w}(\ell) + \boldsymbol{\varepsilon}(\ell), \quad (14)$$

where  $\mathbf{Z}(\ell) = \mathbf{X}(\ell)$  will include the intercept and the three predictors; their varying effect will be represented by  $\mathbf{w}(\ell)$ , which we recover by implementing Q-MGP models. Storing posterior samples of the multivariate spatially-varying coefficients for the full data with  $q = 4$  is impossible using our computing resources as each sample would be of size  $1000 \times 1000 \times 64 \times 4 = 2.56\text{E}+8$ . For this reason, we consider two feasible setups. Denote by  $n_{\text{all}}$  the number of locations, including those corresponding to missing NDVI output. In model (1), we subsample each image to obtain 64 frames of size  $500 \times 500$ , and fit a regression model with  $\mathbf{Z}(\ell) = \mathbf{1}$  resulting in a spatially-varying intercept model on  $n_{\text{obs}} = 12,582,484$  observed locations, a total of  $n_{\text{all}} = 16,000,000$  locations for prediction, and a latent spatial random effect  $\mathbf{w}$  of the same size. The Q-MGP model was fit using  $M = 328,125$  space-time regions of average size  $\sim 48$ .

The base covariance of equation (13) becomes a univariate non-separable spatiotemporal covariance as in Gneiting (2002). In model (2), we aim to estimate the varying effect of elevation on NDVI. We subsample each image to obtain 64 frames of size  $278 \times 278$ , each covering an area of  $25 \times 25$  km, and take  $\mathbf{Z}(\ell) = (\mathbf{1} \ \mathbf{X}_{\text{elev}}(\ell))$  resulting in  $q = 2$  and targeting the recovery of a latent spatial random effect vector of size 9,892,352. Considering the additional computational burden of the multivariate latent effects, in this case we used  $M = 156,800$ , corresponding to smaller space-time regions of average size  $\sim 31$ . In this model there is a single unknown  $\delta_{ij}$  in eq. (13) which corresponds to the latent dissimilarity between the intercept and elevation. We thus consider  $\psi_2 = (a_2\delta_{ij} + 1)^{\beta_2}$  as the unknown parameter. We assign priors  $\beta_r \sim N(0, 100)$  for  $r = 1, \dots, q$ ,  $\sigma^2 \sim \text{Inv.G.}(2, 1)$ ,  $\tau^2 \sim \text{Inv.G.}(2, 1)$ , and uniform priors to other covariance parameters (their support is reported in Table 2).

In both cases, approximate posterior samples of the latent random effects and the other

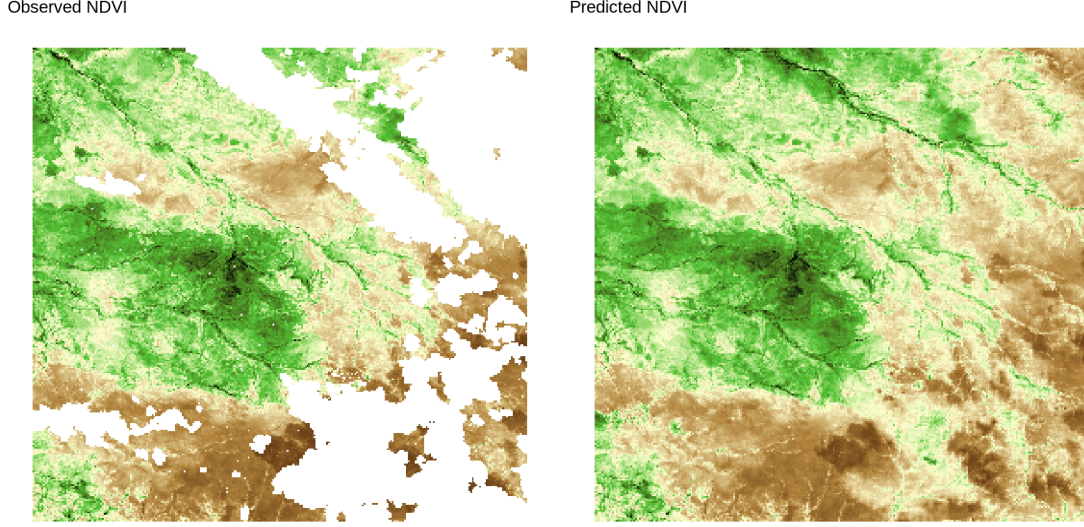
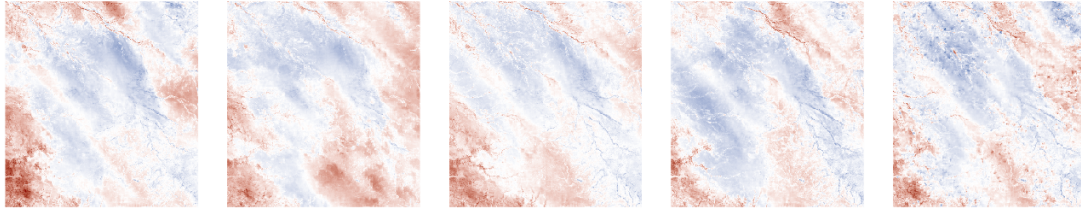


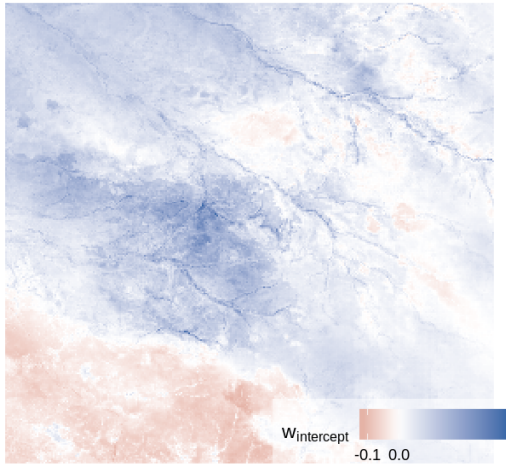
Figure 7: NDVI predictions from Q-MGP model (2) at time 60 (2016-12-17).

unknown parameters were obtained by running the proposed Gibbs sampler for a total of 25,000 iterations. A posterior sample of size 500 was obtained by using the first 22,000 iterations as burn-in, and thinning the remaining 3,000 by a factor of 6. Additional computational details are at Appendix C. Posterior summaries of the unknown parameters for these models are reported in Table 2, along with root mean square error (RMSE) in predicting NDVI at 10,000 left-out locations, 95% posterior coverage at those locations, and run times. Both models achieved similar out-of-sample predictive performance and coverage. Figure 7 shows the NDVI predictions of model (2) at one of the 64 time points. This reveals that the varying effect of elevation on NDVI output is credibly different from zero at 42.54% of the space-time locations (95% c. i.). Figure 8 shows the space-time varying effect of elevation on NDVI. In particular, it highlights the extent to which higher elevation reduces vegetation. In the same figure, we note that the spatial range is approximately 4km; the time range is about 8 days. The large estimated  $\psi_2$  indicates that the estimated correlation between the two covariates of the latent random process is very small at all spatial and temporal lags. The predicted NDVI and latent spatiotemporal effects are available as animated GIF images as part of the supplementary material.

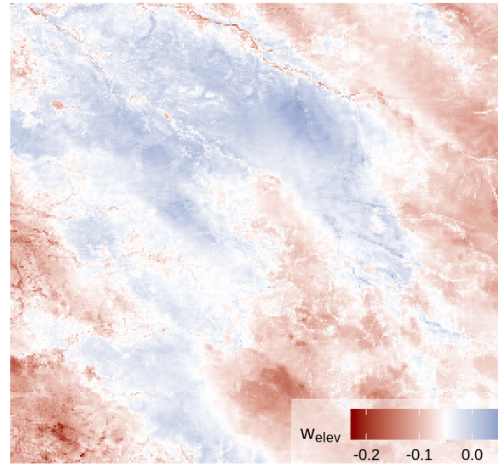
Elevation: effect on NDVI (2016-12-01 to 2017-02-19)



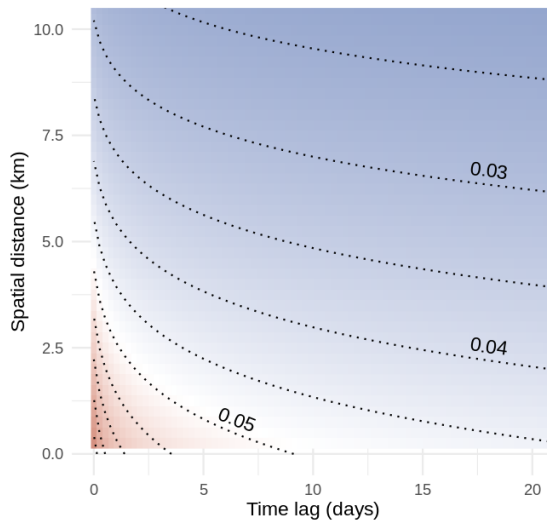
Residual spatial effect



Elevation: effect on NDVI



Covariance with estim. parameters



Elevation: nonzero effect locations (95% cred. int.)

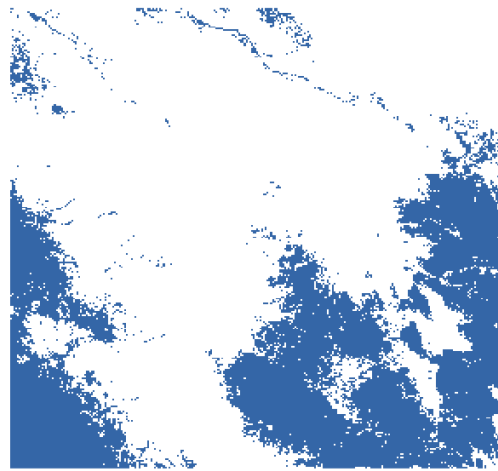


Figure 8: Top: the effect of elevation on NDVI output, evolving over five time periods. Middle left: effect on NDVI not explained by elevation; right: effect on NDVI attributable to elevation. Bottom left: estimated covariance at different space-time lags; right, in blue: locations with credibly nonzero effect of elevation on NDVI output.

	Q-MGP MODEL (1)	Q-MGP MODEL (2)
$n_{\text{all}}$	16,000,000	4,946,176
$n_{\text{obs}}$	12,755,856	3,961,715
$M$	328125	156800
$q$	1	2
$\beta_{\text{elevation}}$	0.0017 <sub>(0.0014,0.0021)</sub>	0.0415 <sub>(0.0398,0.0432)</sub>
$\beta_{\text{topindex}}$	5.54E-4 <sub>(4.72E-4,6.30E-4)</sub>	-0.0011 <sub>(-0.0012,-0.0008)</sub>
$\beta_{\text{accum}}$	-4.84E-4 <sub>(-5.66E-4,-4.02E-4)</sub>	7.88E-4 <sub>(6.94E-4,9.06E-4)</sub>
$\sigma^2$	0.0585 <sub>(0.0583,0.0587)</sub>	0.0728 <sub>(0.0711,0.0749)</sub>
$\tau^2$	1.05E-4 <sub>(1.05E-4,1.05E-4)</sub>	1.27E-4 <sub>(1.21E-4,1.32E-4)</sub>
$c \sim U(0, 1\text{E}+6)$	7.0331 <sub>(7.0146,7.0519)</sub>	3.0710 <sub>(3.0562,3.0846)</sub>
$a_1 \sim U(0, 1\text{E}+6)$	433.98 <sub>(429.67,439.50)</sub>	3857.6 <sub>(3492.6,4154.7)</sub>
$\beta_1 \sim U(0, 1)$	0.0694 <sub>(0.0690,0.0697)</sub>	0.1058 <sub>(0.1043,0.1080)</sub>
$\psi_2 \sim U(0, 1\text{E}+6)$	—	221.36 <sub>(198.09,240.57)</sub>
95% coverage	94.96	95.66
RMSE	0.0175	0.0253
Time/it. (s)	6.18	4.53
Time (hours)	42.9	31.5

Table 2: Posterior summaries of Q-MGP models implemented on the Serengeti data.

## 6 Discussion

We have developed a class of Bayesian hierarchical models for large spatial and spatiotemporal datasets based on linking domain partitions to directed acyclic graphs. These models can be tailored for specific algorithmic needs, and we have demonstrated the advantages of using a cubic tessellation scheme (Q-MGP) when targeting the efficient recovery of spatial random effects in Bayesian hierarchical models using Gibbs samplers.

When considering alternative computational strategies, the proposed Q-MGP may not be optimal. For example, Gaussian first stage models enable marginalization of the latent spatial effects; posterior sampling of unknown covariance parameters via MCMC is typically associated by better mixing. Future research may thus focus on identifying “optimal” DAGs for collapsed samplers. Furthermore, the blocked conditional independence structure of Q-MGPs may be suboptimal as it corresponds to possibly restrictive conditional independence assumptions in neighboring locations. While we have not focused on the effect of different tessellations or partitioning choices in this article, alternative tessellation schemes (e.g. hexagonal) may be associated to less stringent assumptions and possibly better performance,

while retaining all the desirable features of Q-MGP.

Other natural extensions to high-dimensional spatiotemporal statistics include settings where there are a very large number of spatiotemporal outcomes in addition to a large number of spatial and temporal locations. Here there are a few different avenues. One approach is in the same spirit of joint modeling pursued here, but instead of modeling the cross-covariance functions explicitly, as has been done here, we pursue dimension reduction using factor models (see, e.g., [Christensen and Amemiya, 2003](#); [Lopes et al., 2008](#); [Ren and Banerjee, 2013](#); [Taylor-Rodriguez et al., 2019](#)). The aforementioned references have attempted to model the factor models using spatial processes some of which have used scalable low-rank predictive processes or the NNGP. We believe that modeling latent factors using spatiotemporal MGPs will impart some of the computational and inferential benefits seen here. However, this will need further development especially with regard to identifiability of loading matrices ([Lopes et al., 2008](#); [Ren and Banerjee, 2013](#)) and process parameters and should generate relevant questions for future research.

A different approach to multivariate spatial modeling has relied upon conditional or hierarchical specifications. This has been well articulated in the text by [Cressie and Wikle \(2011\)](#); see also [Royle and Berliner \(1999\)](#) and the recent developments in [Cressie and Zammit-Mangion \(2016\)](#). An advantage of the hierarchical approach is that the multivariate processes are valid stochastic processes, essentially by construction and without requiring spectral representations, and can also impart considerable computational benefits. It will be interesting to extend the ideas in [Cressie and Zammit-Mangion \(2016\)](#) to augmented spaces of DAGs to further introduce conditional independence, and therefore sparsity, in MGP models with high-dimensional outcomes.

Finally, it is worth pointing out that alternate computational algorithms, particularly tuned for high-dimensional Bayesian models, should also be explored. Recent developments on algorithms based upon classes of piecewise deterministic Markov processes (see, e.g., [Fearnhead et al., 2018](#); [Bierkens et al., 2019](#), and references therein) that avoid Gibbs samplers and even reversible MCMC algorithms are being shown to be increasingly effective for high-dimensional Bayesian inference. Adapting such algorithms to MGP and Q-MGP for scalable Bayesian spatial process models will constitute natural extensions of our current offering.

## Acknowledgements

Finley and Peruzzi were supported by National Science Foundation (NSF) EF-1253225 and DMS-1916395, and National Aeronautics and Space Administration's Carbon Monitoring System project. Banerjee was supported by NSF DMS-1513654, IIS-1562303, and DMS-1916349.

# Appendix

## A Spatial Meshed Process

Let  $\mathbf{w}(\mathbf{s}), \mathbf{s} \in \mathcal{D}$  be the base process,  $\mathcal{S}$  the fixed reference set,  $\mathcal{L} = \{\ell_1, \dots, \ell_n\} \subset \mathcal{D}$  and  $\mathcal{U} = \mathcal{L} \setminus \mathcal{S}$ . Then the joint density  $\tilde{p}(\mathbf{w}_{\mathcal{L}})$  is proper. In fact, using the definitions of  $\tilde{p}(\mathbf{w}_{\mathcal{S}})$  and  $\tilde{p}(\mathbf{w}_{\mathcal{U}} | \mathbf{w}_{\mathcal{S}})$  we get

$$\begin{aligned} \int \tilde{p}(\mathbf{w}_{\mathcal{L}}) \prod_{\ell_i \in \mathcal{L}} d(\mathbf{w}(\ell_i)) &= \int \int \tilde{p}(\mathbf{w}_{\mathcal{U}} | \mathbf{w}_{\mathcal{S}}) \tilde{p}(\mathbf{w}_{\mathcal{S}}) \prod_{\mathbf{s}_i \in \mathcal{S} \setminus \mathcal{L}} d(\mathbf{w}(\mathbf{s}_i)) \prod_{\ell_i \in \mathcal{L}} d(\mathbf{w}(\ell_i)) \\ &\quad \int \tilde{p}(\mathbf{w}_{\mathcal{U}} | \mathbf{w}_{\mathcal{S}}) \tilde{p}(\mathbf{w}_{\mathcal{S}}) \prod_{\ell_i \in \mathcal{U}} d(\mathbf{w}(\ell_i)) \prod_{\ell_i \in \mathcal{S}} d(\mathbf{w}(\ell_i)) \\ &\quad \int \tilde{p}(\mathbf{w}_{\mathcal{S}}) \left( \int \tilde{p}(\mathbf{w}_{\mathcal{U}} | \mathbf{w}_{\mathcal{S}}) \prod_{\ell_i \in \mathcal{U}} d(\mathbf{w}(\ell_i)) \right) \prod_{\ell_i \in \mathcal{S}} d(\mathbf{w}(\ell_i)) = 1. \end{aligned}$$

We now verify the Kolmogorov consistency conditions. Take  $\mathcal{L}_{\pi} = \{\ell_{\pi(1)}, \dots, \ell_{\pi(n)}\}$  as any permutation of  $\mathcal{L}$ . Then call  $\mathcal{U}_{\pi} = \mathcal{L}_{\pi} \setminus \mathcal{S}$  and we get

$$\tilde{p}(\mathbf{w}_{\mathcal{L}_{\pi}}) = \int \tilde{p}(\mathbf{w}_{\mathcal{U}_{\pi}} | \mathbf{w}_{\mathcal{S}}) \tilde{p}(\mathbf{w}_{\mathcal{S}}) \prod_{\mathbf{s}_i \in \mathcal{S} \setminus \mathcal{L}_{\pi}} d(\mathbf{w}(\mathbf{s}_i)).$$

Set membership is invariant to permutations, so  $\mathcal{U}_{\pi} = \mathcal{L}_{\pi} \setminus \mathcal{S} = \mathcal{L} \setminus \mathcal{S} = \mathcal{U}$ . and therefore in no way the order of the  $\mathcal{L}$  locations changes  $\tilde{p}(\mathbf{w}_{\mathcal{L}})$ . Therefore  $\tilde{p}(\mathbf{w}_{\mathcal{L}_{\pi}}) = \tilde{p}(\mathbf{w}_{\mathcal{L}})$ , i.e.

$$\tilde{p}(\mathbf{w}(\ell_1), \dots, \mathbf{w}(\ell_n)) = \tilde{p}(\mathbf{w}(\ell_{\pi(1)}), \dots, \mathbf{w}(\ell_{\pi(n)})).$$



Next, take another location  $\ell_0 \in \mathcal{D}$ . Call  $\mathcal{L}_1 = \mathcal{L} \cup \{\ell_0\}$ . We want to show that  $\int \tilde{p}(\mathbf{w}_{\mathcal{L}_1}) d(\mathbf{w}(\ell_0)) = \tilde{p}(\mathbf{w}_{\mathcal{L}})$ . If  $\ell_0 \in \mathcal{S}$  then  $\mathcal{L}_1 \setminus \mathcal{S} = \mathcal{L} \setminus \mathcal{S} = \mathcal{U}$  hence

$$\begin{aligned} \int \tilde{p}(\mathbf{w}_{\mathcal{L}_1}) d(\mathbf{w}(\ell_0)) &= \int \tilde{p}(\mathbf{w}_{\mathcal{L}_1 \setminus \mathcal{S}} | \mathbf{w}_{\mathcal{S}}) \tilde{p}(\mathbf{w}_{\mathcal{S}}) \prod_{\mathbf{s}_i \in \mathcal{S} \setminus \mathcal{L}_1} d(\mathbf{w}(\mathbf{s}_i)) d(\mathbf{w}(\ell_0)) \\ &= \int \tilde{p}(\mathbf{w}_{\mathcal{U}} | \mathbf{w}_{\mathcal{S}}) \tilde{p}(\mathbf{w}_{\mathcal{S}}) \prod_{\mathbf{s}_i \in \mathcal{S} \setminus \mathcal{L}} d(\mathbf{w}(\mathbf{s}_i)) = \tilde{p}(\mathbf{w}_{\mathcal{L}}) \end{aligned}$$

If  $\ell_0 \notin \mathcal{S}$

$$\begin{aligned} \int \tilde{p}(\mathbf{w}_{\mathcal{L}_1}) d(\mathbf{w}(\ell_0)) &= \int \left( \int \tilde{p}(\mathbf{w}_{\mathcal{L}_1 \setminus \mathcal{S}} | \mathbf{w}_{\mathcal{S}}) \tilde{p}(\mathbf{w}_{\mathcal{S}}) \prod_{\mathbf{s}_i \in \mathcal{S} \setminus \mathcal{L}_1} d(\mathbf{w}(\mathbf{s}_i)) \right) d(\mathbf{w}(\ell_0)) \\ &= \int \left( \int \tilde{p}(\mathbf{w}_{\mathcal{L} \setminus \mathcal{S} \cup \{\ell_0\}} | \mathbf{w}_{\mathcal{S}}) \tilde{p}(\mathbf{w}_{\mathcal{S}}) \prod_{\mathbf{s}_i \in \mathcal{S} \setminus \mathcal{L}} d(\mathbf{w}(\mathbf{s}_i)) \right) d(\mathbf{w}(\ell_0)) \\ &= \int \left( \int \tilde{p}(\mathbf{w}_{\{\ell_0\}} | \mathbf{w}_{\mathcal{L} \setminus \mathcal{S}}, \mathbf{w}_{\mathcal{S}}) \tilde{p}(\mathbf{w}_{\mathcal{L} \setminus \mathcal{S}} | \mathbf{w}_{\mathcal{S}}) \tilde{p}(\mathbf{w}_{\mathcal{S}}) \prod_{\mathbf{s}_i \in \mathcal{S} \setminus \mathcal{L}} d(\mathbf{w}(\mathbf{s}_i)) \right) d(\mathbf{w}(\ell_0)) \\ &= \int \tilde{p}(\mathbf{w}_{\mathcal{L} \setminus \mathcal{S}} | \mathbf{w}_{\mathcal{S}}) \tilde{p}(\mathbf{w}_{\mathcal{S}}) \prod_{\mathbf{s}_i \in \mathcal{S} \setminus \mathcal{L}} d(\mathbf{w}(\mathbf{s}_i)) \int \tilde{p}(\mathbf{w}_{\{\ell_0\}} | \mathbf{w}_{\mathcal{S}}) d(\mathbf{w}(\ell_0)) \\ &= \int \tilde{p}(\mathbf{w}_{\mathcal{L} \setminus \mathcal{S}} | \mathbf{w}_{\mathcal{S}}) \tilde{p}(\mathbf{w}_{\mathcal{S}}) \prod_{\mathbf{s}_i \in \mathcal{S} \setminus \mathcal{L}} d(\mathbf{w}(\mathbf{s}_i)) \\ &= \tilde{p}(\mathbf{w}_{\mathcal{L}}). \end{aligned}$$

## B Meshed Gaussian Process

In graph  $\mathcal{G}$ , the number of parents of node  $\mathbf{v}_j$  is  $b_j$ , i.e.  $b_j = |\text{Pa}[\mathbf{v}_j]|$ . Therefore  $\mathbf{H}_j = \mathbf{C}_{\mathcal{S}_j, \mathcal{S}_{\text{Pa}[j]}} \mathbf{C}_{\mathcal{S}_{\text{Pa}[j]}}^{-1}$  is a  $qn_j \times q \sum_{r=1}^{b_j} n_r$  matrix which can be partitioned by column in  $b_j$  blocks:

$$\mathbf{H}_j = \left[ \mathbf{H}_{j,1} \mid \cdots \mid \mathbf{H}_{j,b_j} \right],$$

whose  $r$ th block is of size  $q \times q$  and corresponds to the  $r$ th block of  $\mathbf{w}_{\text{Pa}[j]}$ .  $\tilde{p}(\mathbf{w}_{\mathcal{S}}) = \prod_{j=1}^M N(\mathbf{w}_j | \mathbf{H}_j \mathbf{w}_{[j]}, \mathbf{R}_j)$  is then proportional to

$$\frac{1}{\prod_{j=1}^M |\mathbf{R}_j|^{\frac{1}{2}}} \exp \left\{ -\frac{1}{2} \sum_{j=1}^M (\mathbf{w}_j - \mathbf{H}_j \mathbf{w}_{\text{Pa}[j]})^\top \mathbf{R}_j^{-1} (\mathbf{w}_j - \mathbf{H}_j \mathbf{w}_{\text{Pa}[j]}) \right\},$$

and we can define  $\mathbf{H}_j^*$  as the  $qn_j \times qn_{\mathcal{S}}$  matrix such that  $\mathbf{w}_j - \mathbf{H}_j \mathbf{w}_{\text{Pa}[j]} = \mathbf{H}_j^* \mathbf{w}_{\mathcal{S}}$ . Analogously to  $\mathbf{H}_j$ , we can partition  $\mathbf{H}_j^*$  by column in  $M$  blocks,

$$\mathbf{H}_j^* = \left[ \mathbf{H}_{j,1}^* \mid \cdots \mid \mathbf{H}_{j,h}^* \mid \cdots \mid \mathbf{H}_{j,M}^* \right],$$

where each block  $h = 1, \dots, M$

$$\mathbf{H}_{j,h}^* = \begin{cases} \mathbf{O}_{qn_h \times qn_h} & \text{if } \mathbf{v}_h \notin \text{Pa}[\mathbf{v}_j] \\ \mathbf{I}_{qn_j \times qn_j} & \text{if } \mathbf{v}_h = \mathbf{v}_j \\ -\mathbf{H}_{j,r} & \text{if } \mathbf{v}_h \text{ is } \mathbf{v}_j\text{'s } r\text{th parent,} \end{cases}$$

and notice that  $h > j$  implies  $\mathbf{v}_h \notin \text{Pa}[\mathbf{v}_j]$ . Then,

$$\sum_{j=1}^M (\mathbf{w}_j - \mathbf{H}_j \mathbf{w}_{\text{Pa}[j]})^\top \mathbf{R}_j^{-1} (\mathbf{w}_j - \mathbf{H}_j \mathbf{w}_{\text{Pa}[j]}) = \sum_{j=1}^M \mathbf{w}_{\mathcal{S}}^\top \mathbf{H}_j^{*\top} \mathbf{R}_j^{-1} \mathbf{H}_j^* \mathbf{w}_{\mathcal{S}} = \mathbf{w}_{\mathcal{S}}^\top \mathbf{H}_{\mathcal{S}}^{*\top} \mathbf{R}_{\mathcal{S}}^{-1} \mathbf{H}_{\mathcal{S}}^* \mathbf{w}_{\mathcal{S}},$$

where  $\mathbf{H}_{\mathcal{S}}^*$  is a  $qn_{\mathcal{S}} \times qn_{\mathcal{S}}$  block-matrix whose  $j$ th block-row is  $\mathbf{H}_j^*$  for  $j = 1, \dots, M$ , and  $\mathbf{R}_{\mathcal{S}} = \text{blockdiag}(\mathbf{R}_1, \dots, \mathbf{R}_M)$ . The resulting precision matrix  $\tilde{\mathbf{C}}_{\mathcal{S}}^{-1} = \mathbf{H}_{\mathcal{S}}^{*\top} \mathbf{R}_{\mathcal{S}}^{-1} \mathbf{H}_{\mathcal{S}}^*$  is thus a  $qn_{\mathcal{S}} \times qn_{\mathcal{S}}$  matrix made of  $M \times M$  blocks of sizes  $qn_j \times qn_j$  for  $j = 1, \dots, M$  such that  $\sum n_j = n_{\mathcal{S}}$ . We denote its  $(i, j)$  block as  $\tilde{\mathbf{C}}_{\mathcal{S}}^{-1}(i, j)$  and note that by symmetry its transpose is  $(\tilde{\mathbf{C}}_{\mathcal{S}}^{-1}(i, j))^\top = \tilde{\mathbf{C}}_{\mathcal{S}}^{-1}(j, i)$ . We find the nonzero blocks of  $\tilde{\mathbf{C}}_{\mathcal{S}}^{-1}$  in its block-diagonal, and for  $i \neq j$  in the  $(i, j)$  block such that  $\mathbf{v}_i$  and  $\mathbf{v}_j$  are connected in the moralized subgraph  $\mathcal{G}^m(\mathbf{A})$  of  $\mathcal{G}(\mathbf{A})$  obtained by subsetting  $\mathcal{G}$  to the  $\mathbf{A}$  nodes and linking those that share a child; in other words for all  $\mathbf{v}_i, \mathbf{v}_j \in \mathbf{A}$ , either (1)  $\mathbf{v}_i \in \text{Pa}[\mathbf{v}_j]$  or vice-versa, or (2) there exists  $\mathbf{v}_h$  such that  $\{\mathbf{v}_i, \mathbf{v}_j\} \subset \text{Pa}[\mathbf{v}_h]$ . The sparsity of  $\tilde{\mathbf{C}}_{\mathcal{S}}^{-1}$  thus depends on the specific choice for  $\mathcal{G}(\mathbf{A})$  and the corresponding moralized graph  $\mathcal{G}^m(\mathbf{A})$  (Cowell et al., 1999). Suppose that  $\mathcal{G}(\mathbf{A})$  has  $M$  vertices and induces  $\mathcal{G}^m(\mathbf{A})$  whose number of undirected edges is  $k \ll M(M-1)/2$ . This means that the number of “missing” connections is  $\ell = M(M-1)/2 - k$ . Assume that each subset  $\mathcal{S}_j$  of the reference set is of size  $n_j = n/M$ , so that each block of  $\tilde{\mathbf{C}}_{\mathcal{S}}^{-1}$  is of size  $qn/M \times qn/M$ . Then the precision matrix will have  $\ell \left(\frac{qn}{M}\right)^2$  zeros. Given a partition for  $\mathcal{D}$  which induces a partition for  $\mathcal{S}$  into  $M$  disjoint subsets, one can thus increase sparsity in the precision matrix at  $\mathcal{S}$  by choosing a graph which induces a lower  $\ell$ . But note that all nodes linked to locations outside the reference set, i.e. any  $\mathbf{v} \in \mathbf{B}$ , do not influence the precision matrix  $\tilde{\mathbf{C}}_{\mathcal{S}}^{-1}$ .

The covariance function of the new process will then be defined using  $\tilde{\mathbf{C}}$ : consider two locations  $\ell_1$  and  $\ell_2$  in  $\mathcal{D}$ . If both are in  $\mathcal{S}$  then  $\ell_1 = \mathbf{s}_i$ ,  $\ell_2 = \mathbf{s}_j$  for some  $i, j$ , and  $Cov_{\tilde{p}}(\mathbf{w}(\mathbf{s}_i), \mathbf{w}(\mathbf{s}_j)) = \tilde{\mathbf{C}}_{\mathbf{s}_i, \mathbf{s}_j}$ . If  $\ell_1 = \mathbf{u}_i \in \mathcal{U}$  with parents  $\text{Pa}[\eta(\mathbf{u}_i)]$  and  $\ell_2 = \mathbf{s}_j \in \mathcal{S}$  then

$$\begin{aligned} Cov_{\tilde{p}}(\mathbf{w}(\mathbf{u}_i), \mathbf{w}(\mathbf{s}_j)) &= E_{\tilde{p}}(Cov_{\tilde{p}}(\mathbf{w}(\mathbf{u}_i), \mathbf{w}(\mathbf{s}_j) \mid \mathbf{w}_{\mathcal{S}})) + Cov_{\tilde{p}}(E_{\tilde{p}}(\mathbf{w}(\mathbf{u}_i) \mid \mathbf{w}_{\mathcal{S}}), E_{\tilde{p}}(\mathbf{w}(\mathbf{s}_j) \mid \mathbf{w}_{\mathcal{S}})) \\ &= 0 + Cov_{\tilde{p}}(\mathbf{H}_{\mathbf{u}_i} \mathbf{w}_{[\mathbf{u}_i]}, \mathbf{w}(\mathbf{s}_j)) \\ &= \mathbf{H}_{\mathbf{u}_i} \tilde{\mathbf{C}}_{\mathcal{S}_{[\mathbf{u}_i]}, \mathbf{s}_j} \end{aligned}$$

Finally if  $\ell_1 = \mathbf{u}_i \in \mathcal{U}$  and  $\ell_2 = \mathbf{u}_j \in \mathcal{U}$  then

$$Cov_{\tilde{p}}(\mathbf{w}(\mathbf{u}_i), \mathbf{w}(\mathbf{u}_j)) = \delta_{(\mathbf{u}_i = \mathbf{u}_j)} \mathbf{R}_{\mathbf{u}_i} + \mathbf{H}_{\mathbf{u}_i} \tilde{\mathbf{C}}_{\mathcal{S}_{[\mathbf{u}_i]}, \mathcal{S}_{[\mathbf{u}_j]}} \mathbf{H}_{\mathbf{u}_j}^{\top}.$$

## B.1 Choice of $\mathcal{S}$ and $\mathcal{U}$

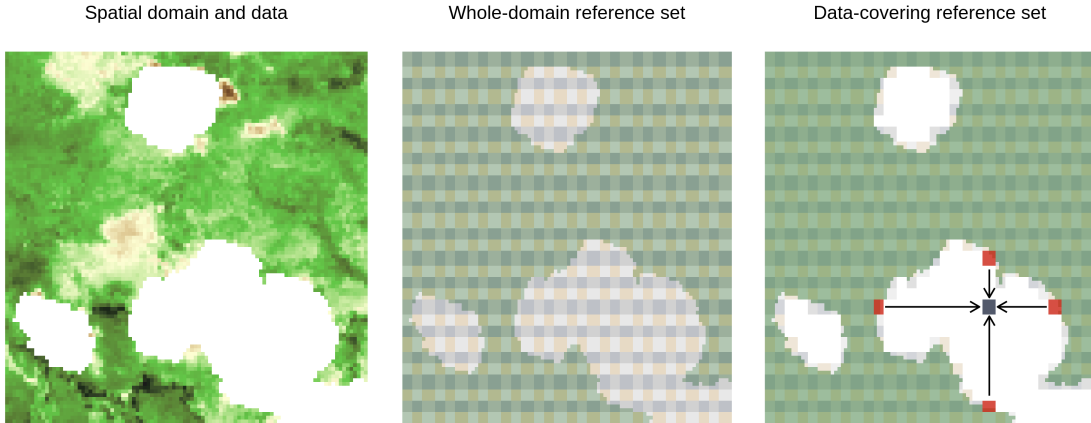


Figure 9: Reference sets

The two sets of locations  $\mathcal{S}$  and  $\mathcal{U}$  differ in that the former is linked to nodes  $\mathbf{A}$  of graph  $\mathcal{G}$ , whereas the latter is linked to nodes  $\mathbf{B}$  with no children. Since  $\mathbf{B}$  nodes are independent of each other given realizations of  $\mathbf{A}$  they provide little information on spatial dependence; in fact, the set  $\mathcal{S}$  is akin to the set of knots in a predictive process model. Unlike those models,  $\mathcal{S}$  can be chosen to be as large as the set of observations, and  $\mathcal{U}$  left empty. Generally, it is possible to choose  $\mathcal{S} \supset \mathcal{T}$  to smoothly model spatial dependence across larger regions of unobserved locations, but convergence of the Gibbs sampler may be slower at locations that

are very far from the nearest observed ones. Therefore, a convenient choice which is possibly safer for MCMC convergence is to let them coincide, i.e.  $\mathcal{S} = \mathcal{T}$ .

Matters are less straightforward when redundancies occur. Consider locations  $\mathbf{t} = (t_1, \dots, t_d) \in \mathcal{D}$  such that  $t_j = t_j^* \delta_j$  where  $t_j^* = 1, \dots, N_j$  and  $\delta_j \in [0, 1/N_j]$  for  $j = 1, \dots, d$ . Denote the set of such locations as  $\mathcal{T}^*$ ; this is a  $N_1 \times \dots \times N_d$  grid of equally-spaced locations. If observed locations are on a quantized grid of coordinates, i.e. there are  $\{t_j^*, \delta_j\}_{j=1}^d$  such that  $\mathcal{T} \subset \mathcal{T}^*$ , choosing  $\mathcal{S} = \mathcal{T}$  may be inefficient as it may reduce the number of redundant  $\mathbf{R}_j$ 's and thus increase computation time. Instead, choosing  $\mathcal{S}$  such that  $\mathcal{T} \subset \mathcal{S} \subset \mathcal{T}^*$  (possibly  $\mathcal{S} = \mathcal{T}^*$ ) may be much more efficient.

In Figure 9 we show how a small subsample of a time slice of the Serengeti data. Large portions of the spatial domain are missing, but observed locations are at quantized coordinates. We may thus choose to extend  $\mathcal{S}$  to the whole domain (Fig. 9, center) or to extend it just enough to cover all observed locations (Fig. 9, right). For predictions, in the former case we use samples from the full conditional distribution  $p(\mathbf{w}_j \mid \mathbf{w}_{-j}, \mathcal{D})$ . In the latter case, we map empty blocks to nodes  $\mathbf{B}$ : predictions thus easily proceed in parallel since nodes  $\mathbf{B}$  are independent of each other given nodes in  $\mathbf{A}$ , with  $\text{Pa}[\mathbf{b}]$  being composed of the nearest  $\mathbf{A}$  nodes along each axis-parallel direction.

## C C++ implementation of Q-MGP in meshgp

All applications were run on a 512GB-memory, dual-CPU server with two Intel Xeon E5-2699v3 processors, each with 18 cores at 2.3Ghz each, running Debian linux and R version 3.6 linked to the OpenBLAS libraries. Source code for implementing Q-MGP models is available as R package `meshgp` ( [github.com/mkln/meshgp](https://github.com/mkln/meshgp) ). The `meshgp` package is written in Armadillo (Sanderson and Curtin 2016, a C++ library for linear algebra) which can easily be linked to high performance libraries. Parallelization of all high-dimensional operations is implemented via OpenMP (Dagum and Menon, 1998). R packages `Rcpp` (Eddelbuettel and François, 2011) and `RcppArmadillo` (Eddelbuettel and Sanderson, 2014) are used for interfacing the C++ source with R.

## D Comparisons with methods in [Heaton et al. \(2019\)](#)

In recent work, [Heaton et al. \(2019\)](#) have reviewed and compared 13 state-of-the-art models for large spatial datasets in a predictive challenge involving (1) simulated and (2) real-world spatial data (daytime land surface temperatures as measured by the Terra instrument onboard the MODIS satellite on August 4, 2016, Level-3 data). The two datasets are available at [github.com/finnlindgren/heatoncomparison](https://github.com/finnlindgren/heatoncomparison). The total number of locations is the same in both cases ( $n_{\text{all}} = 150,000$ ), with the goal of predicting outcomes when missing. Both datasets include  $n_{\text{train}} = 105,569$  available locations; the test set is of size  $n_{\text{test}} = 44,431$  for the simulated data,  $n_{\text{test}} = 42,740$  for the MODIS data due to cloud cover.

We estimate two MGP models for each dataset by partitioning the spatial domain into  $M = 1500$  (resp. 375) rectangular regions for an average block size of 100 (resp. 400) spatial locations, and fix  $\mathcal{G}$  as a cubic mesh. We assign blocks to  $\mathcal{S}$  to cover the observed locations; the remaining ones will be used for prediction as in the right plot of Figure 9. Finally, we use an exponential base covariance function. We ran our Gibbs sampler using  $\sigma^2 \sim \text{Inv.Gamma}(2.01, 1)$ ,  $\tau^2 \sim \text{Inv.Gamma}(2.01, 1)$ ,  $\phi \sim U[1/10, 30]$  as priors, and respectively 10, 1, 10 as starting values. A log-Normal proposal function was used for the Metropolis update of  $\phi$ . We ran a total of 6,000 Monte Carlo iterations, with 4,000 dropped as burn-in, and thinning 2:1 the remaining ones to obtain a sample of size 1,000 that approximates the joint posterior distribution  $p(\mathbf{w}, \phi, \sigma^2, \tau^2 \mid \mathbf{y})$  which we then use to obtain predictions. In both cases, the algorithm ran on 40 threads. We report the results of our analysis in Table 3, whereas prediction plots for both datasets are in Figure 10.

We also report results from select models tested in [Heaton et al. \(2019\)](#) to facilitate comparisons. Refer to the cited work for a more in-depth overview. We selected: nearest-neighbor Gaussian process (NNGP), conjugate ([Finley et al., 2019](#)) and response ([Datta et al., 2016a](#)) algorithms; the multiresolution approximation (MRA) model of [Katzfuss \(2017\)](#); a stochastic partial differential equations (SPDE) approach estimated via integrated nested Laplace approximations ([Rue et al., 2009](#); [Lindgren et al., 2011](#)); metakriging ([Guhaniyogi and Banerjee, 2018](#)).

In terms of predictive performance, coverage, and computation time, both implemented models are competitive with the top-ranking ones in [Heaton et al. \(2019\)](#). In particular, our

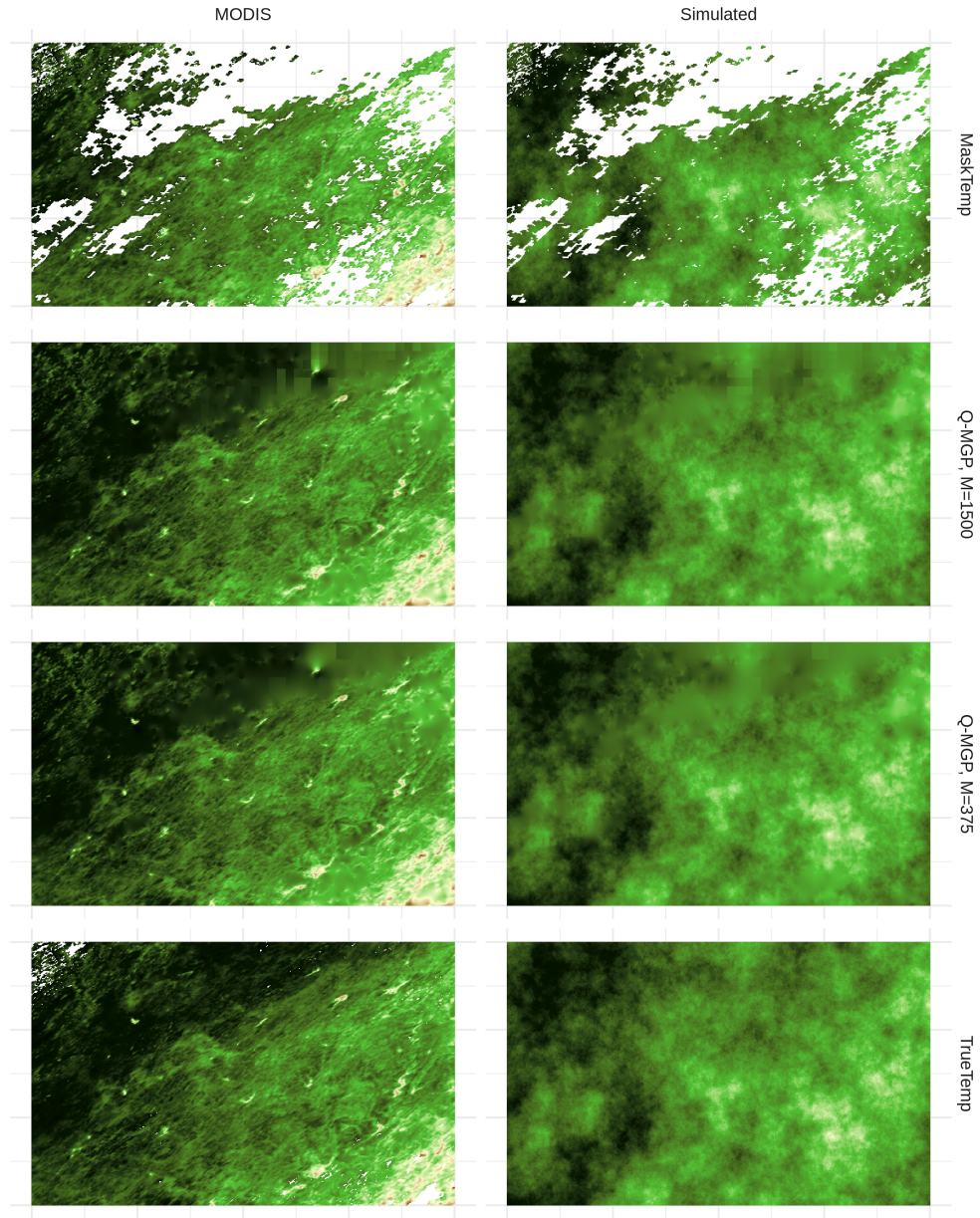


Figure 10: Spatial data and predicted temperatures for Q-MGP models. Top: grey areas correspond to missing observations. Middle rows: spatial predictions. Bottom: the true outcomes. Left: MODIS data; right: simulated data.

Simulated data	MAE	RMSE	Coverage	Run Time	N. Cores	Code Lang.
Q-MGP, $M = 1500$	0.6270	0.8721	<b>95.46</b>	16.4 min	40	C++ (Armadillo)
Q-MGP, $M = 375$	<b>0.6136</b>	0.8407	<b>95.62</b>	133.2 min	40	C++ (Armadillo)
NNGP Conjugate	0.65	0.88	96	1.99 min	10	C++
NNGP Response	0.65	0.88	96	45.56 min	10	C++
MRA	<b>0.61</b>	<b>0.83</b>	93	13.57 min	1	Matlab
SPDE	0.62	0.86	100	138.34 min	2	R ( <b>inla</b> )
Metakriging	0.74	97	99	2888.89 min	30	R ( <b>spBayes</b> )

MODIS data	MAE	RMSE	Coverage	Run Time	N. Cores	Code Lang.
Q-MGP, $M = 1500$	1.1151	1.5598	<b>95.14</b>	16.5 min	40	C++ (Armadillo)
Q-MGP, $M = 375$	<b>1.0729</b>	<b>1.5034</b>	<b>95.20</b>	133.7 min	40	C++ (Armadillo)
NNGP Conjugate	1.21	1.64	<b>95</b>	2.06 min	10	C++
NNGP Response	1.24	1.68	94	42.85 min	10	C++
MRA	1.33	1.85	92	15.61 min	1	Matlab
SPDE	1.10	1.53	97	120.33 min	2	R ( <b>inla</b> )
Metakriging	2.08	2.50	89	2888.52 min	30	R ( <b>spBayes</b> )

Table 3: Comparative performance of Q-MGP and select methods in [Heaton et al. \(2019\)](#).



approach (with  $M = 1500$ ) is much faster than Bayesian models estimated via MCMC – note that *NNGP Conjugate* uses cross-validation to select suitable covariance parameters. The slower alternative with  $M = 375$  – corresponding to a much coarser partitioning, i.e. larger regions – was possible by caching the redundant matrix operations given that the data are on a regular lattice. We chose  $M = 375$  by targeting a total computing time similar to the SPDE model, which achieved the lowest predictive error in the MODIS dataset. Computing times should not differ dramatically on a dual-CPU Intel Xeon server as in [Heaton et al. \(2019\)](#).

## E Caching algorithm

**Input:**  $\Gamma = \{\Gamma_i\}_{i=1}^g$ : a collection of matrices of size  $n_{\Gamma_i} \times d$  for  $i = 1, \dots, g$ . Each row is denoted  $\Gamma_i[\mathbf{r}, :]$  for  $r = 1, \dots, n_{\Gamma_i}$ .

**for**  $i \in \{1, \dots, g\}$  **do**

- Sort  $\Gamma_i$  using column 1; resolve ties using columns 2 to  $d$ .
- Calculate  $\Gamma_{0,i}$  as the matrix of size  $n_{\Gamma_i} \times d$  such that
$$\Gamma_{0,i}[\mathbf{r}, :] = \Gamma_i[1, :] \text{ for } r = 1, \dots, n_{\Gamma_i}.$$
- Calculate  $\tilde{\Gamma}_i = \Gamma_i - \Gamma_{0,i}$ .

**end**

**Initialize:**  $\Delta_\Gamma = \{\delta_1, \dots, \delta_g\}$  where  $\delta_i = i$  for all  $i = 1, \dots, g$ .

**for**  $i \in \{1, \dots, g\}$  **do**

**for**  $j \in \{1, \dots, i\}$  **do**

**if**  $\tilde{\Gamma}_i = \tilde{\Gamma}_j$  (*element by element*) **then**  
        |     Set  $\delta_i = j$ .

**end**

**end**

**Output:**  $\Delta_\Gamma$ : a dictionary with  $g$  keys and  $g^*$  unique values. If  $f$  is a function such that  $f(\Gamma + t) = f(\Gamma)$  then  $f(\Gamma_{\delta_i}) = f(\Gamma_j)$  for all  $i$  such that  $\delta_i = j$ .

**Algorithm 1:** Caching algorithm.

Algorithm 1 can be used by taking  $\Gamma = \{(\mathcal{S}_j, \mathcal{S}_{[j]})\}_{j=1:M}$  for  $\mathbf{C}_{\mathcal{S}_j, \mathcal{S}_{[j]}}$ ,  $\Gamma = \{\mathcal{S}_j\}_{j=1:M}$

for  $\mathbf{C}_{\mathcal{S}_j}$ , and  $\mathbf{\Gamma} = \{\mathcal{S}_{[j]}\}_{j=1:M}$  for  $\mathbf{C}_{\mathcal{S}_{[j]}}^{-1}$ . The resulting dictionaries can be used to build a dictionary  $\Delta_{\mathbf{R}}$  for  $\{\mathbf{R}_j\}_{j=1:M}$  with  $M^*$  unique values. Each iteration of the Gibbs sampler becomes cheaper if the number of unique values in  $\Delta_{\mathbf{R}}$  is  $M^* \ll M$ .

## F Benefits of MGPs on tessellated domains

The block conditional independence structure of tessellated MGPs favors parallelization and MCMC mixing; when data are on semi-regular lattices, using standard base covariance functions results in regular patterns and many redundant expensive matrix operations can be avoided. We now show the practical benefits of this class of models using a cubic MGP design.

### F.1 Compute time with caching and parallelization

As we mentioned earlier, our approach enables parallelization of all high-dimensional operations and facilitates caching if locations are at least in part on a regular grid. Figure 11 shows the time-per-iteration of Q-MGP, on a fully-observed slice of the Serengeti data,  $n = 1,000,000$ , choosing  $M \in \{150^2, 250^2\}$ , and with or without caching.  $M = 250^2$  corresponds to blocks with 16 locations (all blocks are of dimension  $4 \times 4$ ), whereas  $M = 150^2$  to blocks of dimension 36, 42, 49 corresponding to squares of size  $6 \times 6, 6 \times 7$  or  $7 \times 6, 7 \times 7$ , respectively. Note that caching is optional; in this case we showcase the speed differential between best-case (regular lattice) and worst-case (completely irregularly-spaced observations) scenarios by disabling caching.

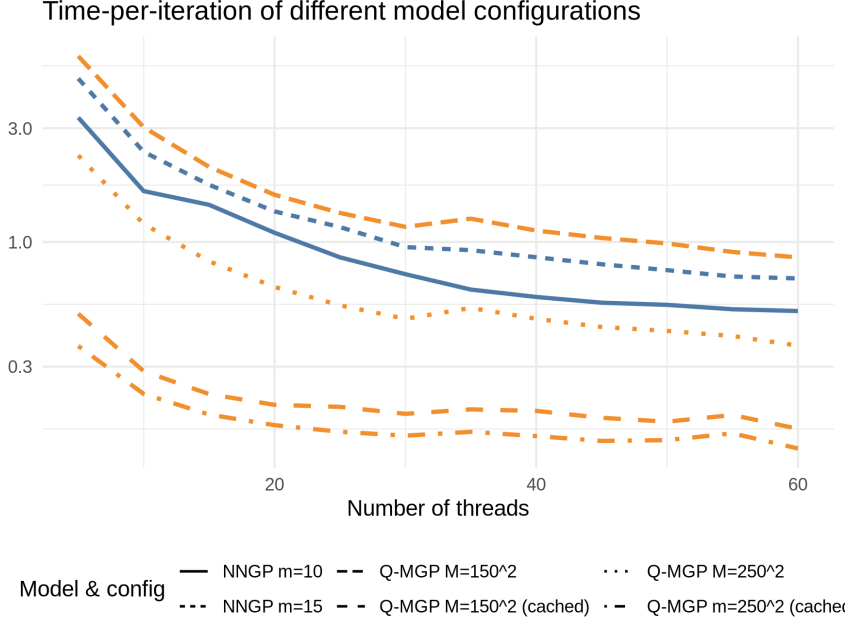


Figure 11: Computation time per iteration, in logarithmic scale, of Q-MGP and NNGP at different configurations.

To put the numbers in perspective, we compare our results with NNGP models estimated via the sequential sampler of [Datta et al. \(2016a\)](#) as implemented in the highly optimized R package `spNNGP`, choosing  $m \in \{10, 15\}$ . Like our method, this alternative is fully Bayesian, recovers the spatial random effects, and is estimated via a Gibbs sampler. Unlike Q-MGP, it does not use caching or sample  $\mathbf{w}$  in parallel. Computing times of Q-MGP models without caching are comparable to NNGP models; the Q-MGP model with block size 16 is about 30% faster than the NNGP model with 10 neighbors.

However, caching allows one to consider much larger regions at little additional computation cost: without caching, the large-region Q-MGP model ( $M = 150^2$ ) is about 2.5 times slower than its small-region counterpart ( $M = 250^2$ ). With caching turned on, the small-region model is only 25% faster, and the large-region one is still about 4 times faster than NNGP with  $m = 10$ . Similarly, the large savings in computing time induced by using caching in Q-MGP models allowed us to design the best-performing model for the real-world application of [Heaton et al. \(2019\)](#), see Table 3.

There is little evidence of marked advantages specifically due to parallel sampling with this 60-core virtual machine, other than a seemingly slightly steeper downward slope for the

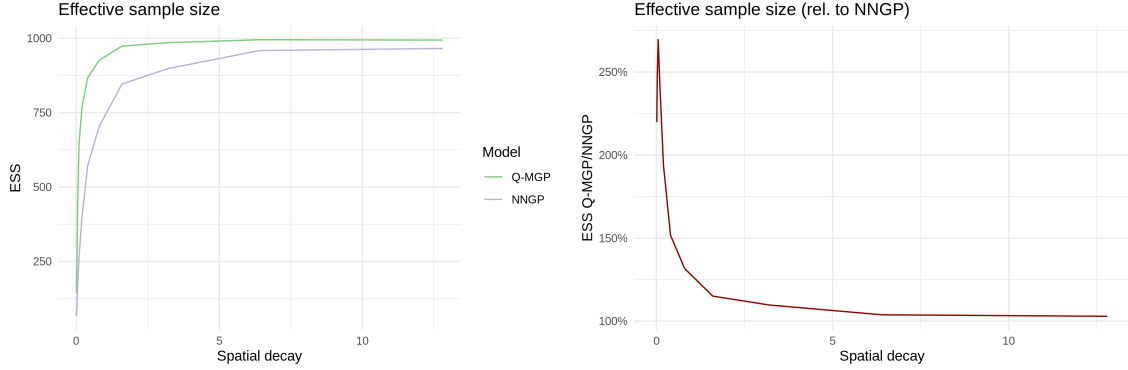


Figure 12: Effective sample size (ESS) of Q-MGP and NNGP for different values of the spatial exponential decay parameter  $\phi$ .

computing time of the non-cached Q-MGP models towards the right of Figure 11, possibly indicating an unexploited potential speedup with a greater number of cores; this may be an area for future research.

## F.2 Effective sample size of MCMC posterior samples

After convergence, Markov-chain Monte Carlo algorithms output correlated samples from the posterior distribution, and their efficiency is decreased when successive samples are highly autocorrelated. In these settings, one needs a much larger MCMC sample size to reliably summarize posterior information. When memory is limited, one “thins” the chain and only stores one posterior sample every  $T$  MCMC iterations. For a given correlated posterior sample, one can measure this phenomenon via the effective sample size (ESS), which is the size of an independent sample equivalent to the correlated sample at hand. Highly autocorrelated Markov chains result in lower ESS. This scenario arises in geostatistical settings with large-scale spatial dependency, as the high-dimensional latent spatial random effects are highly correlated at nearby locations. For this reason, Gibbs samplers such as the one proposed in this article and the sequential NNGP sampler of [Datta et al. \(2016a\)](#) are expected to be negatively affected by slowly-decaying spatial correlation.

With this in mind, we now compare the parallel sampler of Q-MGPs to a sequential NNGP sampler (from R package `spNNGP`, [Finley et al. 2020](#)) in terms of ESS of the latent random effects. We generate  $\mathbf{y} = \mathbf{Z}\mathbf{w} + \boldsymbol{\varepsilon}$  on a regular  $80 \times 80$  grid where  $\mathbf{Z} = \mathbf{I}_n$ ,  $n = 6400$ , the spatial process is  $\mathbf{w} \sim GP(0, \mathbf{C})$ ,  $\mathbf{C}(\|\mathbf{h}\|) = \sigma^2 \exp\{-\phi\|\mathbf{h}\|\}$  for  $\mathbf{h} = \boldsymbol{\ell}' - \boldsymbol{\ell}$ ,  $\boldsymbol{\varepsilon}(\boldsymbol{\ell}) \sim N(0, \tau^2)$

for all  $\ell$  and using parameters  $\sigma^2 = 1$  and  $\phi \in \{0.01, 0.025, 0.05, .1, .2, .4, .8, 1.6, 3.2, 6.4, 12.8\}$ , and nugget  $\tau^2 = 0.01$ . The goal is to sample  $\mathbf{w}$  a posteriori. We assign priors  $\phi \sim U[.01, 30]$ ,  $\sigma^2 \sim \text{Inv.G.}(2.01, 1)$ ,  $\tau^2 \sim \text{Inv.G.}(2.01, 1)$  and use the true values of  $\{\sigma^2, \phi, \tau^2\}$  as starting values for the Gibbs sampler of both NNGP and Q-MGP. The starting value of  $\mathbf{w}$  was set to a vector of zeros of size  $n$ . We let the Markov chain run for a total of 2000 iterations, discarding the first 1000. The NNGP model used  $m = 10$  neighbors, whereas the Q-MGP model used  $M = 270$  regions obtained by axis-parallel partitioning the spatial domain along the two dimensions into 15 and 18 intervals, respectively. We chose  $M = 270$  to achieve about the same computation time when caching was disabled (actual Q-MGP run times were about 2.6 to 3 times faster than NNGP-sequential once caching was turned on). Figure 12 shows the effective sample size of the resulting approximated posterior sample of  $\mathbf{w}$ , averaged across all spatial locations. While both models evidence a degradation of performance with long-range spatial dependence (small  $\phi$ ), the NNGP model shows significantly worse performance. With low spatial decay, the Q-MGP model exhibits effective sample sizes up to 2.5 times larger than the equivalent NNGP model. The smaller effective sample size of NNGPs implies that a much larger number of MCMC samples would be necessary to appropriately approximate an independent posterior sample of size 1000, resulting in significantly longer “effective” compute times. We estimate Q-MGP models to be up to ten times faster than sequential NNGPs. As expected, given the small sample size, the differences reduce for larger values of  $\phi$ , in which case both models output posterior samples with small autocorrelation with large ESS. Larger data sizes are generally associated to worse mixing so we expect these findings to be generalizable to those settings.

## G Recovering missing pixels of an animated GIF image

Lion GIF	MAE	RMSE	Coverage (90%)
Q-MGP, $M = 1050$	<b>0.0341</b>	<b>0.0715</b>	<b>93.28</b>
Gapfill	0.0480	0.0923	62.76

Table 4: Comparative performance of Q-MGP and Gapfill on recovering missing pixels of an animated GIF image.

We compare Q-MGPs with Gapfill (Gerber et al., 2018) on non-Gaussian data in the form of an animated GIF image. The original GIF image collects 30 frames, each of size  $200 \times 250$ , for a total data size of 1.5 million locations. We subsample the data size to  $n_{\text{all}} = 94,500$  by downsampling each of the 30 frames at a 16:1 ratio. Similarly to Section 5.2, we simulate cloud cover by placing random clouds in 5 of the 30 frames, covering all but 10 locations in 5 of 30 frames, and covering 50% random locations in 5 of the 30 frames; 15 frames were thus untouched. See Figure 13. The resulting dataset includes  $n_{\text{obs}} = 67,363$  non-missing observations and  $n_{\text{test}} = 27,137$  missing ones to be predicted. We implement a Q-MGP model with  $M = 1050$  found by partitioning the spatial coordinates into 5 and 21 intervals, and time in 10 intervals. We run the Gibbs sampler for 15000 iterations; we discard the first 10000 and keep one every five of the remaining 5000 to obtain a sample of size 1000 from the approximated posterior distribution, which we use for predictions. We used the same base covariance, prior distributions, and starting values as in previous sections, for a total run time of 35 minutes (0.14s/iteration) on 11 threads. As seen in Table 4 and from a visual inspection of Figure 13, Q-MGP outperforms Gapfill.

## References

- Apanasovich, T. V. and Genton, M. G. (2010). Cross-covariance functions for multivariate random fields based on latent dimensions. *Biometrika*, 97:15–30. [doi:10.1093/biomet/asp078](https://doi.org/10.1093/biomet/asp078). 21
- Banerjee, S. (2017). High-dimensional Bayesian geostatistics. *Bayesian Analysis*, 12(2):583–614. [doi:10.1214/17-BA1056R](https://doi.org/10.1214/17-BA1056R). 2
- Banerjee, S. (2020). Modeling Massive Spatial Datasets Using a Conjugate Bayesian Linear Modeling Framework. *Spatial Statistics*, in press. [doi:10.1016/j.spasta.2020.100417](https://doi.org/10.1016/j.spasta.2020.100417). 7
- Banerjee, S., Finley, A. O., Waldmann, P., and Ericsson, T. (2010). Hierarchical spatial process models for multiple traits in large genetic trials. *Journal of American Statistical Association*, 105(490):506–521. [doi:10.1198/jasa.2009.ap09068](https://doi.org/10.1198/jasa.2009.ap09068). 2
- Banerjee, S., Gelfand, A. E., Finley, A. O., and Sang, H. (2008). Gaussian predictive process

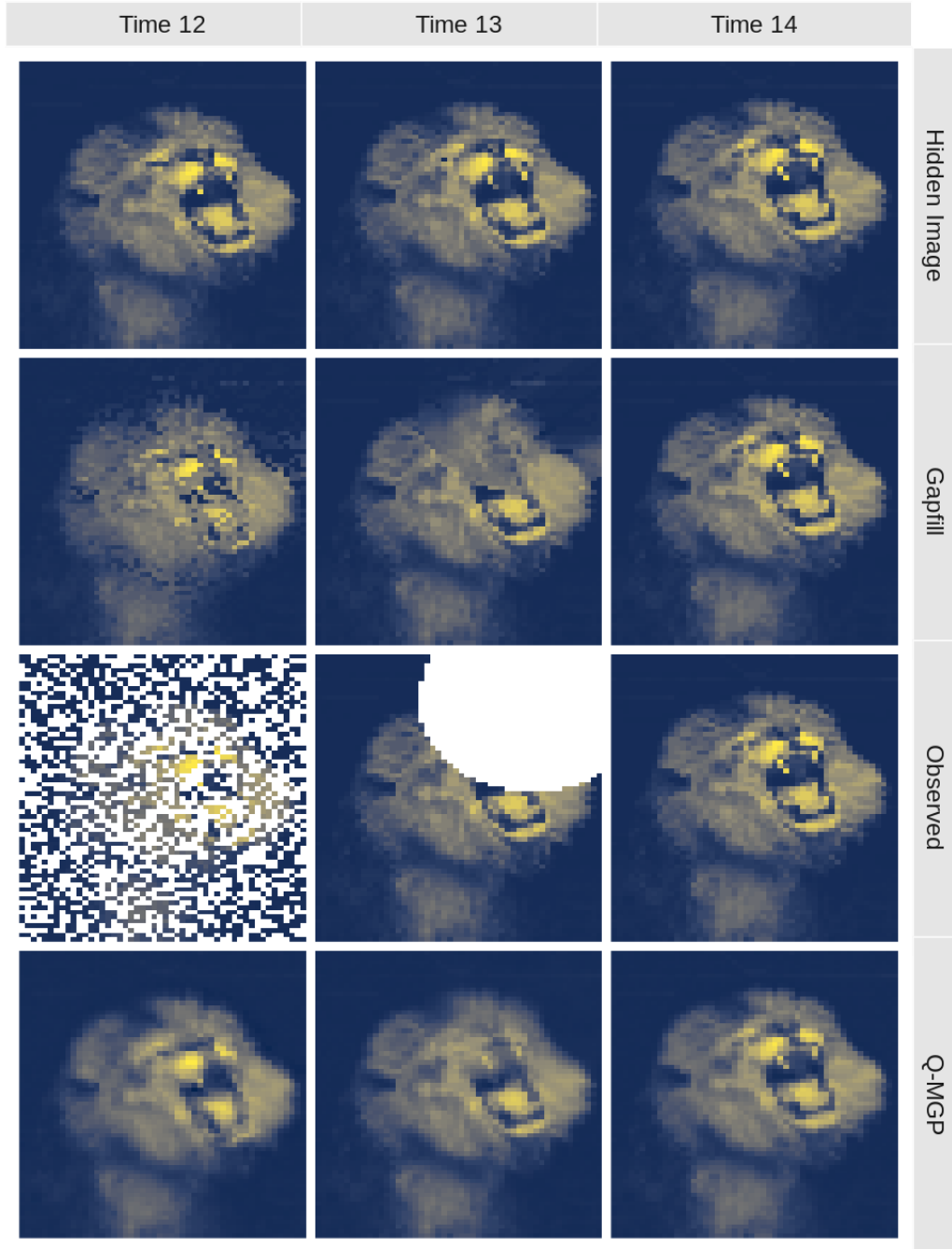


Figure 13: From the top: full original image frames to be recovered, predictions by Q-MGP and Gapfill, and observed image frames, at three select times (of 30 total) of the GIF image.

- models for large spatial data sets. *Journal of the Royal Statistical Society, Series B*, 70:825–848. doi:10.1111/j.1467-9868.2008.00663.x. 2
- Bierkens, J., Fearnhead, P., and Roberts, G. (2019). The zig-zag process and super-efficient sampling for bayesian analysis of big data. *Ann. Statist.*, 47(3):1288–1320. 28
- Chen, Y., Davis, T. A., Hager, W. W., and Rajamanickam, S. (2008). Algorithm 887: CHOLMOD, Supernodal Sparse Cholesky Factorization and Update/Downdate. *ACM Trans. Math. Softw.*, 35(3). doi:10.1145/1391989.1391995. 11
- Christensen, W. F. and Amemiya, Y. (2003). Modeling and prediction for multivariate spatial factor analysis. *Journal of Statistical Planning and Inference*, 115(2):543 – 564. doi:10.1016/S0378-3758(02)00173-8. 28
- Cowell, R. G., Dawid, A. P., Lauritzen, S. L., and Spiegelhalter, D. J. (1999). *Probabilistic Networks and Expert Systems*. Springer-Verlag, New York. 31
- Cressie, N. and Johannesson, G. (2008). Fixed Rank Kriging for Very Large Spatial Data Sets. *Journal of the Royal Statistical Society, Series B*, 70:209–226. doi:10.1111/j.1467-9868.2007.00633.x. 2
- Cressie, N. and Zammit-Mangion, A. (2016). Multivariate spatial covariance models: a conditional approach. *Biometrika*, 103(4):915–935. doi:10.1093/biomet/asw045. 28
- Cressie, N. A. C. and Wikle, C. K. (2011). *Statistics for spatio-temporal data*. Wiley series in probability and statistics. Hoboken, N.J. Wiley. 28
- Dagum, L. and Menon, R. (1998). OpenMP: an industry standard api for shared-memory programming. *Computational Science & Engineering, IEEE*, 5(1):46–55. 33
- Datta, A., Banerjee, S., Finley, A. O., and Gelfand, A. E. (2016a). Hierarchical nearest-neighbor gaussian process models for large geostatistical datasets. *Journal of the American Statistical Association*, 111:800–812. doi:10.1080/01621459.2015.1044091. 3, 6, 34, 39, 40
- Datta, A., Banerjee, S., Finley, A. O., Hamm, N. A. S., and Schaap, M. (2016b). Nonseparable dynamic nearest neighbor gaussian process models for large spatio-temporal data with an application to particulate matter analysis. *The Annals of Applied Statistics*, 10:1286–1316. doi:10.1214/16-AOAS931. 3



- Davis, T. A. (2006). *Direct Methods for Sparse Linear Systems*. SIAM, Philadelphia, PA. doi:10.1137/1.9780898718881. 11
- Desanker, G., Dahlin, K. M., and Finley, A. O. (2019). Environmental controls on landsat-derived phenoregions across an east african megatransect. *Ecosphere*, In press. 23
- Eddelbuettel, D. and François, R. (2011). Rcpp: Seamless R and C++ integration. *Journal of Statistical Software*, 40(8):1–18. doi:10.18637/jss.v040.i08. 33
- Eddelbuettel, D. and Sanderson, C. (2014). RcppArmadillo: Accelerating R with high-performance C++ linear algebra. *Computational Statistics and Data Analysis*, 71:1054–1063. doi:10.1016/j.csda.2013.02.005. 33
- Eidsvik, J., Shaby, B. A., Reich, B. J., Wheeler, M., and Niemi, J. (2014). Estimation and prediction in spatial models with block composite likelihoods. *Journal of Computational and Graphical Statistics*, 23:295–315. doi:10.1080/10618600.2012.760460. 3
- Fearnhead, P., Bierkens, J., Pollock, M., and Roberts, G. O. (2018). Piecewise deterministic markov processes for continuous-time monte carlo. *Statistical Science*, 33(3):386–412. doi:10.1214/18-STS648. 28
- Finley, A. O., Banerjee, S., and Gelfand, A. E. (2012). Bayesian dynamic modeling for large space-time datasets using gaussian predictive processes. *Journal of Geographical Systems*, 14:29–47. doi:10.1007/s10109-011-0154-8. 2
- Finley, A. O., Datta, A., and Banerjee, S. (2020). R package for Nearest Neighbor Gaussian Process models. arXiv:2001.09111. 40
- Finley, A. O., Datta, A., Cook, B. D., Morton, D. C., Andersen, H. E., and Banerjee, S. (2019). Efficient Algorithms for Bayesian Nearest Neighbor Gaussian Processes. *Journal of Computational and Graphical Statistics*, 28:401–414. doi:10.1080/10618600.2018.1537924. 4, 11, 34
- Furrer, R., Genton, M. G., and Nychka, D. (2006). Covariance Tapering for Interpolation of Large Spatial Datasets. *Journal of Computational and Graphical Statistics*, 15:502–523. doi:10.1198/106186006X132178. 2
- Genton, M. G. and Kleiber, W. (2015). Cross-Covariance Functions for Multivariate Geostatistics. *Statistical Science*, 30:147–163. doi:10.1214/14-STS487. 9

- Gerber, F., Furrer, R., Schaepman-Strub, G., de Jong, R., and Schaepman, M. E. (2018). Predicting missing values in spatio-temporal remote sensing data. *IEEE Transactions on Geoscience and Remote Sensing*, 56(5):2841–2853. doi:[10.1109/TGRS.2017.2785240](https://doi.org/10.1109/TGRS.2017.2785240). 22, 42
- Gneiting, T. (2002). Nonseparable, Stationary Covariance Functions for Space-Time Data. *Journal of the American Statistical Association*, 97:590–600. doi:[10.1198/016214502760047113](https://doi.org/10.1198/016214502760047113). 21, 24
- Gonzalez, J., Low, Y., Gretton, A., and Guestrin, C. (2011). Parallel gibbs sampling: From colored fields to thin junction trees. In Gordon, G., Dunson, D., and Dudík, M., editors, *Proceedings of the Fourteenth International Conference on Artificial Intelligence and Statistics*, volume 15 of *Proceedings of Machine Learning Research*, pages 324–332, Fort Lauderdale, FL, USA. PMLR. 19
- Gramacy, R. B. and Apley, D. W. (2015). Local Gaussian Process Approximation for Large Computer Experiments. *Journal of Computational and Graphical Statistics*, 24:561–578. doi:[10.1080/10618600.2018.1537924](https://doi.org/10.1080/10618600.2018.1537924). 6
- Gramacy, R. B. and Lee, H. K. H. (2008). Bayesian Treed Gaussian Process Models With an Application to Computer Modeling. *Journal of the American Statistical Association*, 103:1119–1130. doi:[10.1198/016214508000000689](https://doi.org/10.1198/016214508000000689). 4
- Guhaniyogi, R. and Banerjee, S. (2018). Meta-kriging: Scalable bayesian modeling and inference for massive spatial datasets. *Technometrics*, 60(4):430–444. doi:[10.1080/00401706.2018.1437474](https://doi.org/10.1080/00401706.2018.1437474). 34
- Guhaniyogi, R., Finley, A. O., Banerjee, S., and Gelfand, A. E. (2011). Adaptive Gaussian predictive process models for large spatial datasets. *Environmetrics*, 22:997–1007. doi:[10.1002/env.1131](https://doi.org/10.1002/env.1131). 2
- Guinness, J. (2018). Permutation and grouping methods for sharpening gaussian process approximations. *Technometrics*, 60(4):415–429. doi:[10.1080/00401706.2018.1437476](https://doi.org/10.1080/00401706.2018.1437476). 3, 6, 7
- Heaton, M. J., Datta, A., Finley, A. O., Furrer, R., Guinness, J., Guhaniyogi, R., Gerber, F., Gramacy, R. B., Hammerling, D., Katzfuss, M., Lindgren, F., Nychka, D. W., Sun, F., and Zammit-Mangion, A. (2019). A case study competition among methods for analyzing large spatial data. *Journal of Agricultural, Biological and Environmental Statistics*, 24(3):398–425. doi:[10.1007/s13253-018-00348-w](https://doi.org/10.1007/s13253-018-00348-w). 21, 34, 36, 37, 39

- Katzfuss, M. (2017). A multi-resolution approximation for massive spatial datasets. *Journal of the American Statistical Association*, 112:201–214. doi:[10.1080/01621459.2015.1123632](https://doi.org/10.1080/01621459.2015.1123632). 3, 4, 34
- Katzfuss, M. and Guinness, J. (2017). A general framework for Vecchia approximations of Gaussian processes. [arXiv:1907.10109](https://arxiv.org/abs/1907.10109). 3, 6
- Kaufman, C. G., Schervish, M. J., and Nychka, D. W. (2008). Covariance Tapering for Likelihood-Based Estimation in Large Spatial Data Sets. *Journal of the American Statistical Association*, 103:1545–1555. doi:[10.1198/016214508000000959](https://doi.org/10.1198/016214508000000959). 2
- Lauritzen, S., L. (1996). *Graphical Models*. Clarendon Press, Oxford, UK. 7
- Lindgren, F., Rue, H., and Lindstr  m, J. (2011). An explicit link between Gaussian fields and Gaussian Markov random fields: the stochastic partial differential equation approach. *Journal of the Royal Statistical Society: Series B*, 73:423–498. doi:[10.1111/j.1467-9868.2011.00777.x](https://doi.org/10.1111/j.1467-9868.2011.00777.x). 34
- Lopes, H. F., Salazar, E., and Gamerman, D. (2008). Spatial dynamic factor analysis. *Bayesian Analysis*, 3(4):759 – 792. doi:[10.1214/08-BA329](https://doi.org/10.1214/08-BA329). 28
- Quiroz, Z. C., Prates, M. O., and Dey, D. K. (2019). Block Nearest Neighbor Gaussian processes for large datasets. [arXiv:1604.08403](https://arxiv.org/abs/1604.08403). 4
- Ren, Q. and Banerjee, S. (2013). Hierarchical factor models for large spatially misaligned data: A low-rank predictive process approach. *Biometrics*, 69(1):19–30. doi:[10.1111/j.1541-0420.2012.01832.x](https://doi.org/10.1111/j.1541-0420.2012.01832.x). 28
- Royle, J. A. and Berliner, L. M. (1999). A hierarchical approach to multivariate spatial modeling and prediction. *Journal of Agricultural, Biological, and Environmental Statistics*, pages 29–56. 28
- Rue, H. and Held, L. (2005). *Gaussian Markov Random Fields: Theory and Applications*. Chapman & Hall/CRC. doi:[10.1007/978-3-642-20192-9](https://doi.org/10.1007/978-3-642-20192-9). 3
- Rue, H., Martino, S., and Chopin, N. (2009). Approximate Bayesian inference for latent Gaussian models by using integrated nested Laplace approximations. *Journal of the Royal Statistical Society: Series B*, 71:319–392. doi:[10.1111/j.1467-9868.2008.00700.x](https://doi.org/10.1111/j.1467-9868.2008.00700.x). 34

- Sanderson, C. and Curtin, R. (2016). Armadillo: a template-based C++ library for linear algebra. *Journal of Open Source Software*, 1:26. [33](#)
- Sang, H. and Huang, J. Z. (2012). A full scale approximation of covariance functions for large spatial data sets. *Journal of the Royal Statistical Society, Series B*, 74:111–132. [doi:10.1111/j.1467-9868.2011.01007.x](#). [2](#)
- Stein, M. L. (2014). Limitations on low rank approximations for covariance matrices of spatial data. *Spatial Statistics*, 8:1–19. [doi:doi:10.1016/j.spasta.2013.06.003](#). [3](#)
- Stein, M. L., Chi, Z., and Welty, L. J. (2004). Approximating likelihoods for large spatial data sets. *Journal of the Royal Statistical Society, Series B*, 66:275–296. [doi:10.1046/j.1369-7412.2003.05512.x](#). [6](#)
- Sun, Y., Li, B., and Genton, M. (2011). Geostatistics for large datasets. In Montero, J., Porcu, E., and Schlather, M., editors, *Advances and Challenges in Space-time Modelling of Natural Events*, pages 55–77. Springer-Verlag, Berlin Heidelberg. [doi:10.1007/978-3-642-17086-7](#). [2](#)
- Taylor-Rodriguez, D., Finley, A. O., Datta, A., Babcock, C., Andersen, H. E., Cook, B. D., Morton, D. C., and Banerjee, S. (2019). Spatial factor models for high-dimensional and large spatial data: An application in forest variable mapping. *Statistica Sinica*, 29(3):1155–1180. [doi:10.5705/ss.202018.0005](#). [28](#)
- Vecchia, A. V. (1988). Estimation and model identification for continuous spatial processes. *Journal of the Royal Statistical Society, Series B*, 50:297–312. [doi:10.1111/j.2517-6161.1988.tb01729.x](#). [3](#), [4](#), [6](#)
- Yannakakis, M. (1981). Computing the minimum fill-in is NP-Complete. *SIAM Journal on Algebraic and Discrete Methods*, 2(1):77–79. [doi:10.1137/0602010](#). [14](#)